Graphite as a core material for generation IV nuclear reactors

B J Marsden, A N Jones, G N Hall, M Treifi and P M Mummery
The University of Manchester, Nuclear Graphite Research Group

Introduction

Along with the use of carbon coated uranium oxide fuel articles [1], the use of graphite as a moderator for Generation VI reactors is attractive because it allows a reactor core to be designed in a way which, in fault conditions, can reach high enough temperatures to allow the "Doppler effect" [2] to come into play which will shut down the reactor. Such a design does not require operator actions or electronic feedback to safely shut down the reactor in the event of a loss of coolant incident and can be considered to be passively nuclear safe.

The two main Generation IV graphite moderated designs include the Very High Temperature Reactors (VHTR or HTR) and the Molten Salt Reactor (MSR). Both of these reactor designs are at present, 2016, being developed in China, USA and Europe [3,4]. HTR designs use helium as a coolant gas, therefore radiolytic oxidation [5], which leads to loss of moderator mass in Magnox Reactors and Advance Gas-cooled Reactors (AGRs) is not a design issue. Radiolytic oxidation is also not an issue for MSR [6] which uses molten salt as both a fuel and coolant, however in these designs the infiltration of the salts, and gaseous fission products such as Xenon, into the porous graphite structure has to be considered. MSR also operates at near ambient pressure unlike HTRs and AGRs which all operate at around 40-70bar to improve heat transfer.

Nuclear graphite was first chosen as a moderator in fission reactors because it has a reasonably high scattering cross-section and a low absorbent cross-section, 5.551barn and 0.0035barn, respectively [7]. It also has good structural strength and can be easily machined into the complex shapes required to form graphite cores. Thermally, graphite has a high thermal conductivity, low thermal expansivity and has a very high sublimation temperature, ~4000K, so it will not exhibit phase change. Graphite is not susceptible to thermal shock and in the event of a loss of coolant accident the mass of a graphite core acts as a thermal sink extending thermal transient times to many hours in length giving ample time for safety related remedial actions to take place. Graphite is also thermally stable, i.e. to thermally oxidise graphite it needs to be crushed into small centimetre cubes and to be subjected to high temperatures whilst being blasted with significant amount of oxygen [8], conditions which are not applicable to a Generation IV reactor design.

During reactor operation, fast neutron irradiation significantly changes both the graphite component dimensions and the graphite material properties [9,10]. Of paramount interest to the reactor designer are the dimensional change and the property changes such as the Young's modulus, strength, thermal conductivity and thermal expansivity. These dimensional and property changes can lead to the generation of graphite component thermal and shrinkage stresses [11]. Fortunately these stresses are mostly relieved by irradiation creep. However, there will be residual stresses that are not relieved by the irradiation creep mechanisms, which could challenge the component integrity.

This chapter presents and discusses:

i) Nuclear graphite grades, their manufacture, microstructure and properties
ii) Nuclear graphite irradiation induced dimensional and property changes
iii) The present state of understanding of the microstructural mechanisms of irradiation damage
iv) The background to property models
v) Prediction of the structural integrity of graphite components
vi) Thermal oxidation in fault conditions
vii) Methods for dealing with irradiated graphite waste
viii) Specific issues related Molten Salt Reactors

Nuclear graphite grades, their manufacture, microstructure and properties

Nuclear graphite is an artificially produced polycrystalline material with around 20% porosity [12]. The raw materials and manufacture route used to produce nuclear graphite is basically the same as that used to manufacture graphite electrodes and graphite components used in the electronic industry. The raw materials used are a graphitisable pitch or petroleum coke along with a pitch based binder and pitch based impregnating medium.

Coke is chosen based on its structural isotropy, graphitisabilty and purity. The coke is firstly calcined to remove volatiles, then ground to various particle sizes and graded. The finer material is often referred to as 'flour'. A mixture of coke and flour is then mixed with a pitch binder, the final mixture may consist of in excess of ~80% coke/flour and 20% binder. The mixture is then formed into billets, often referred to as the "green articles". As well as the choice of raw materials, the method of forming largely defines the product final properties. Methods used include extrusion and various moulding/pressing methods. Forming methods of particular interest to the nuclear engineer are extrusion, vibration moulding and iso-moulding. Iso-moulding involves the use of a rubber bag into which the coke/binder mixture is contained whilst a hydrostatic pressure is applied externally to obtain a near isotropic product. Early reactor cores tended to be manufactured using readily available pure anisotropic graphite billets. However, modern reactors call for near isotropic graphite grades which can be produced using all three forming methods described above. However, the degree of isotropy may vary.

The green article is then baked in a thermal cycle reaching around 800^{o}C that may last many days. The billets now are referred to as baked carbon, which is often used in the steel industry as a furnace liner but is unsuitable for nuclear application. Baking is followed by an impregnation stage. To aid impregnation the surface of the billets may then be ground to break the surface layer to allow better access for the impregnation pitch. The billets are then placed in an autoclave under vacuum and the impregnation pitch added; the billets are re-baked. This process may be repeated one or two times; however, the improvement in properties becomes less and less with each subsequent re-impregnation.

The next stage is graphitisation which is carried out either in an Acheson graphitization furnace [12] or in a longitudinal graphitisation furnace. In either case the billets are covered with a thick layer of metallurgic coke to prevent oxidation. A relatively low voltage but large electric current is passed through the stack in order to heat the billet in a graphitisation cycle which will normally reach a temperature of ~2800^{o}C, again taking several days.

If high purity graphite is required there may be another cycle in which the stack is heated to ~2400^{o}C within a halogen atmosphere. It is important to avoid the use of chlorine gas as any chlorine residue could be activated leading to the production of ^{36}Cl which has a very long half-life which in turn has to be accounted for when disposing irradiated graphite waste. The manufacturing process is illustrated in Figure 1.

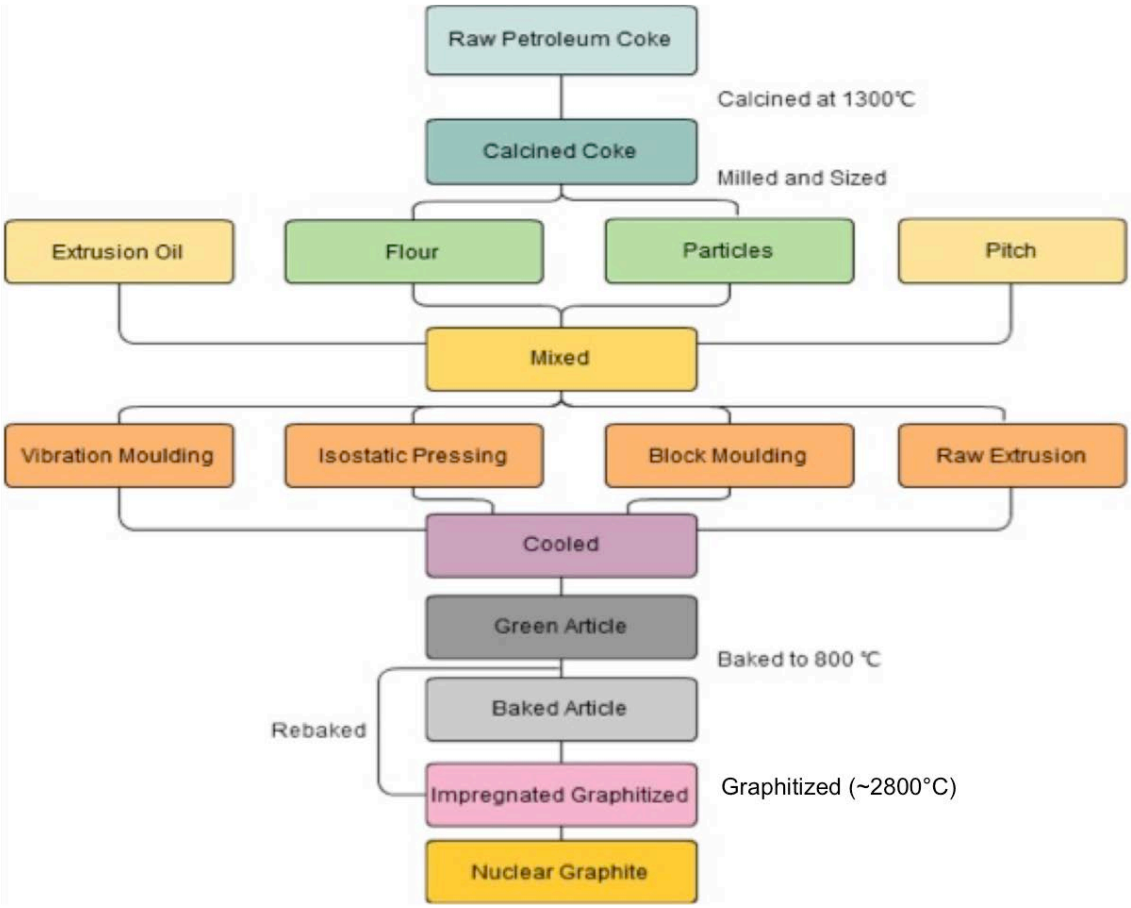

Figure 1 **Nuclear graphite manufacturing route**

The final products are highly pure, porous, polycrystalline graphite billets. Porosity is around 20% and purity is measured in parts volume-per-million. The filler, binder and porosity phases are illustrated in the SEM image given in Figure 2 for medium grained extruded graphite. Transmission electron micrographs demonstrating the basal planes and Mrozowski cracks [13] in a medium grade graphite are shown in Figure 3.

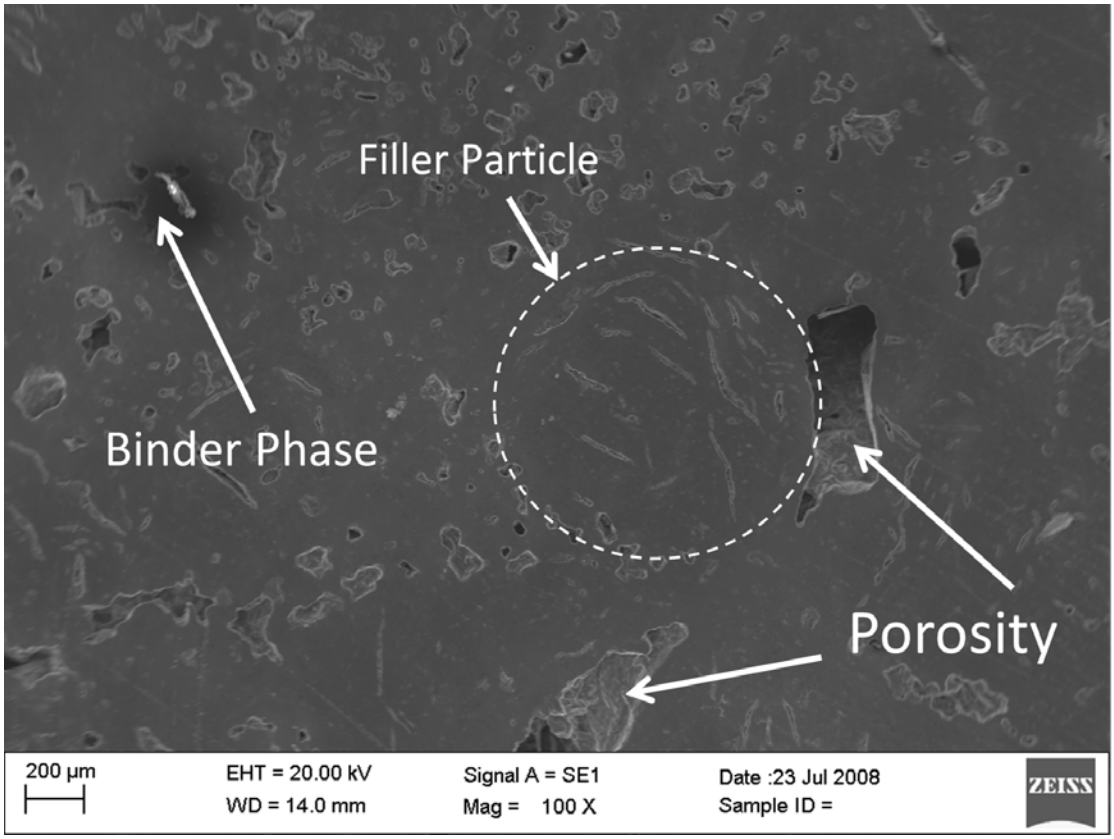

Figure 2 **Graphite grade MG-2 showing filler and binder phases**

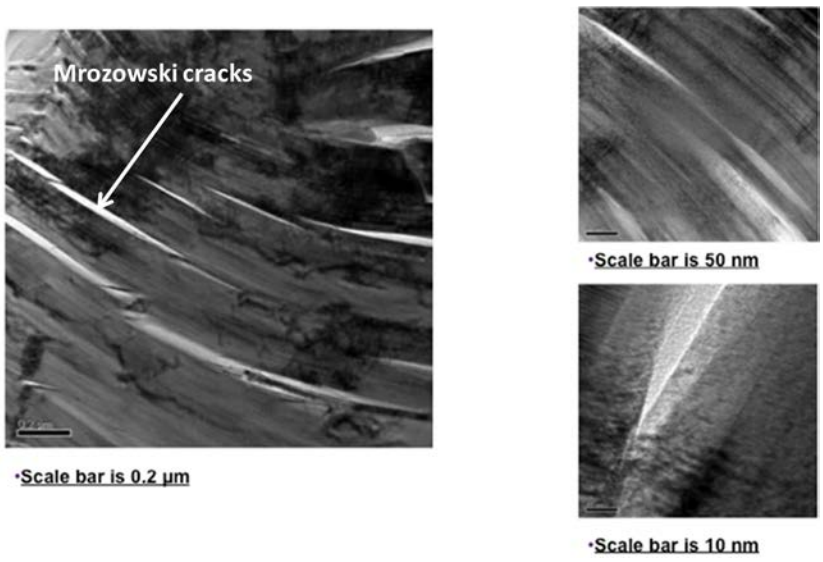

Figure 3 **TEM images of Mrozowski cracks [13] and basal planes**

The graphite crystal structure illustrated in Figure 4 is highly anisotropic, for example Young's modulus in the *c*-axis, C_{11} = 3.46 x 10^{10} N.m^{-2}, whilst in the *a*-axis, C_{33} = 106 x 10^{10} N.m^{-2}. Thus the orientation of the crystallites within the microstructure, along with their distribution will significantly influence the bulk graphite properties. Thus, it is important to choose a coke in which the crystallites are randomly aligned. TEM images of graphite atomic structure are given in Figure 5.

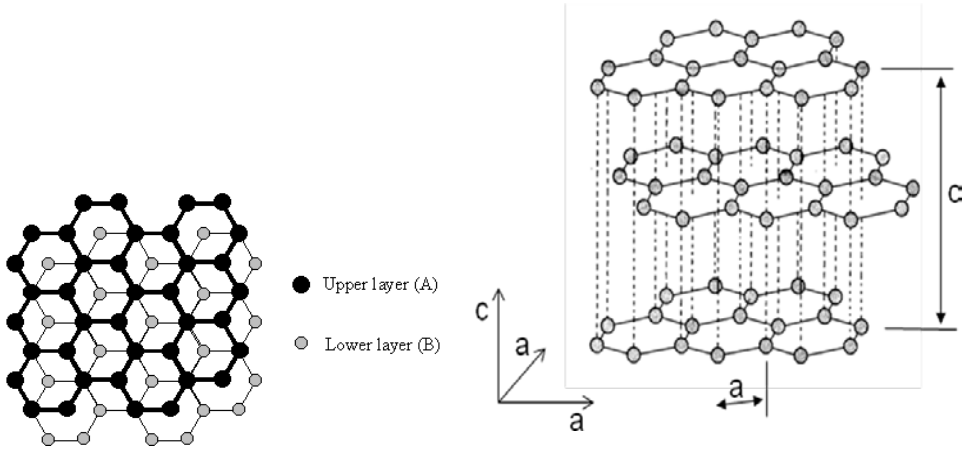

Figure 4 **Graphite crystal structure**

As discussed above the extrusion or moulding method used to form the graphite billets inevitably leads to some bias in the alignment of the filler particles and, hence, the graphite crystallites which are highly anisotropic. The anisotropic bulk properties of the billets are defined by reference to two main directions:

- With Grain (WG) for the direction in which most of crystals '*a*'-axes are aligned.
- Against Grain (AG) for the direction in which most of the crystallite '*c*'-axes are aligned.

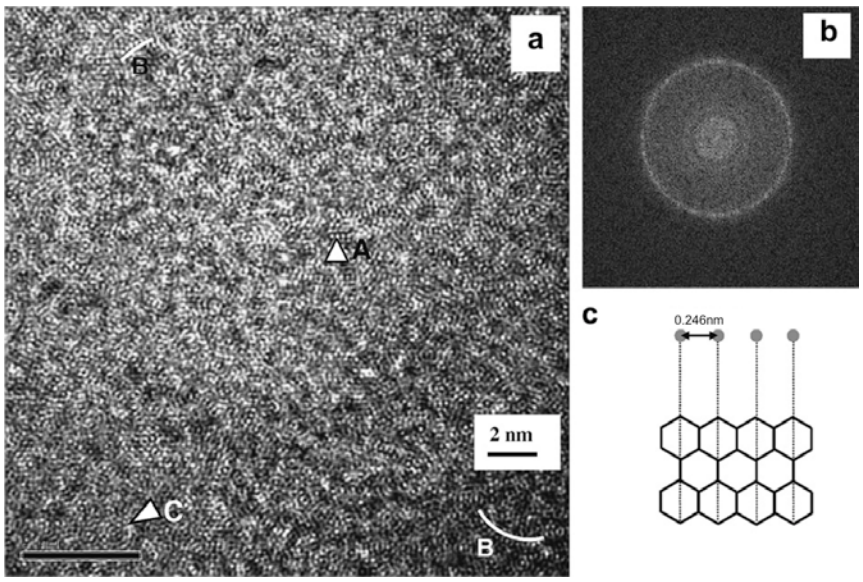

Figure 5 **a) TEM micrograph showing the atomic structure of nuclear graphite via c-axis, b) Selective area diffraction showing lattice parameters and c) atomistic model of graphite layer spacing**

The anisotropy ratio is defined in two ASTM standards, ASTM D7219 and C709-9, [14,15]. Isotropic nuclear graphite is defined as graphite in which the isotropy ratio based on the coefficient of thermal expansion measured over the range (25–500°C) is 1.00–1.10. Near-isotropic nuclear graphite is defined as graphite in which the isotropy based on the coefficient of thermal expansion measured over the range (25–500°C) is 1.10–1.15. In the same standards, the grain size is defined as given in Table 1. Nuclear graphite is usually medium or fine grain although superfine graphite has been considered for MSR applications; polarised optical images of their microstructure are given in Figure 7.

Grain	Definition
Coarse	containing grains in the starting mix that are substantially greater than 4 mm in size
Medium	containing grains in the starting mix that are generally less than 4 mm in size
Fine	containing grains in the starting mix that are generally less than 100 µm in size
Superfine	containing grains in the starting mix that are generally less than 50 µm in size
Ultrafine	containing grains in the starting mix that are generally less than 10 µm in size
Microfine	containing grains in the starting mix that are generally less than 2 µm in size

Table 1 **Polycrystalline graphite grain definition**

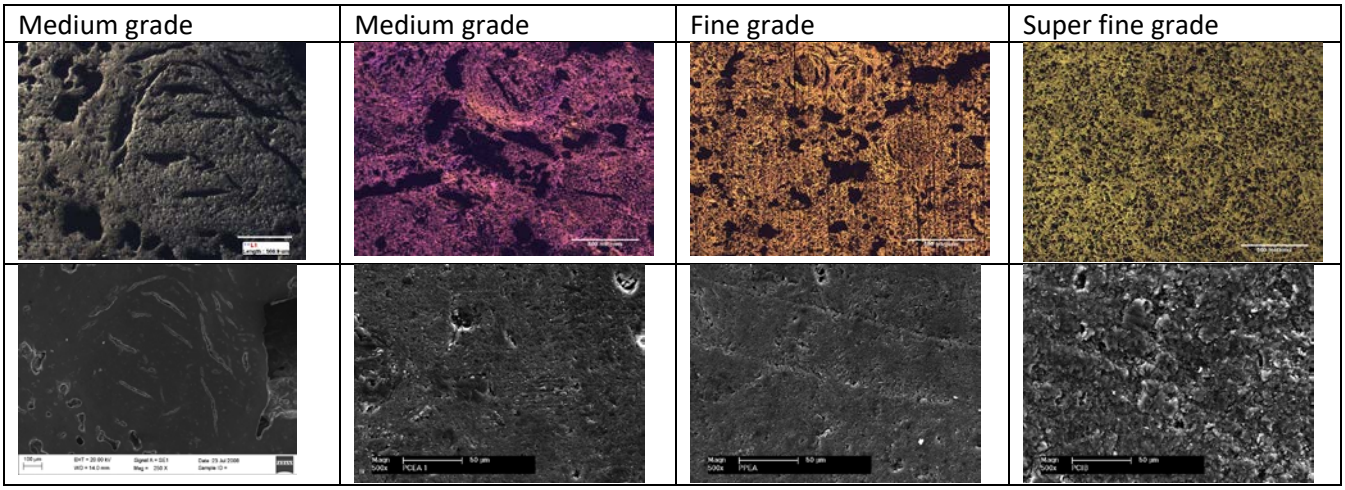

Figure 6 **Polarised Optical micrographs (top) and Scanning electron Micrographs of candidate HTR graphite grades**

Typical unirradiated properties of three nuclear graphite grades are given in Table 2. With increasing temperature, above about 600°C, there is an increase in Young's modulus and strength which is not of importance to lower temperature graphite moderated reactors such as AGRs but should be accounted for when designing HTR graphite cores. Mean CTE increases with temperature and thermal conductivity decreases, again both of these need accounting for when assessing HTR core performance.

Property	Graphite Grade		
	MG-2	**FG-2**	**Gilsocarbon**
Coke	Petroleum	Petroleum	Gilsonite
Grain size μm	300	10	500
Forming method	Extrusion	Iso-moulded	Moulded (Pressing)
Density g/cm^3	1.802	1.77	1.8
Young's modulus GPa - WG	10.7	9.8	10.9
Young's modulus GPa - AG			10.8
Flexural strength MPa - WG	27	39.2	26.9
Flexural strength MPa - AG			26.7
Compressive strength MPa - WG	60	78.4	70.0
Compressive strength MPa - AG			70.0
Tensile strength MPa - WG	19.2	24.5	20.3
Tensile strength MPa - AG			19.9
Coefficient of thermal expansion x10^{-6} K^{-1} [20-120^{o}C] – WG	4.4	3.7	4.7
Coefficient of thermal expansion x10^{-6} K^{-1} [20-120^{o}C] - AG			4.9
Isotropic ratio based on CTE ratio	1.02	Near isotropic	1.04
Thermal conductivity W/mK - WG	146	116	137.9
Thermal conductivity W/mK - AG			137.9

Table 2 **Typical virgin graphite properties**

Nuclear graphite irradiation induced dimensional and property changes

Irradiation fluence units

Historically, within the literature, there is a variety of irradiation units used to describe the aging of graphite due to fast neutron irradiation [10]. Some of the units are based on the burn-up of fuel adjacent to the graphite sample or component. Others are based on the activation of metal foils such as cobalt or Nickel. Yet, other units are based on neutron energy above a certain level.

The main mechanism which drives the irradiation induced changes in nuclear graphite is the displacement of atoms within the crystal structure. Using the latest nuclear data and modern computer codes, it is now possible to calculate carbon atom displacement rates. For this reason it is now preferred that irradiated graphite property change should be related to "displacements per atom per second" (dpa/s) as a flux rate or as "displacements per atom" (dpa) as a fluence; the latter unit being the time integral of the former.

For Generation IV applications, graphite flux and fluence units the reader is likely to encounter are Equivalent Dido Nickel (Flux) Dose (EDNF and EDND) and E>0.18 MeV. The historic unit, EDNF or EDND, arises because much of the UK graphite data was obtained by irradiating small samples in the DIDO material test reactor at Harwell. The unit is defined by Equation 1 as:

$$\text{Equivalent DIDO Flux at point of interest} = \phi_{Ni} = \frac{\phi_{Ni(s)}\phi_d}{\phi_{ds}} \ \text{n/cm}^2\text{/s} \qquad 1$$

where ϕ_{ds} is displacement rate of carbon atoms at the standard position in DIDO (5.25 x 10^{-8} dpa/s), $\phi_{Ni(S)}$ is the integrated flux measured by the nickel activation reaction at the standard position in DIDO (4 x 10^{13} n/cm^2/s) and ϕ_d is displacement rate of carbon atoms at the position of interest. Thus, EDNF = dpa/s/(1.313 x10^{-21}) [10].

Energy above 0.18MeV unit arises from the observation that the integral given in Equation 2 is invariant of reactor design [16].

$$\phi_{(E>E_1)} = \frac{\int_0^\infty \phi(E)\sigma(E)\nu(E)dE}{\int_{E_1}^\infty \phi(E)dE} \qquad 2$$

Equation 2 is essentially the dpa/s at the point of interest divided by the integral of the neutron flux at the same point above energy E1. Various values of E_1 have been used, but for graphite 0.18MeV is the accepted value. Because this unit depends to some extent on the reactor design, the accepted conversion factor of 0.67 used to convert units of E>0.18 to EDNF(D) has some uncertainty associated with it. Conversion factors between the different units are given in Table 3.

Unit	To convert to EDND multiply by
E_n>0.18 MeV (n/cm^2)	0.67
dpa (atom/atom)	7.6162 x 10^{20}

Table 3 **Graphite damage fluence conversion factors**

Irradiated material property data

In this section, irradiated material property data is illustrated with reference to a historic graphite grade, Gilsocarbon, which although no longer available it has an extensive irradiation database. In addition, irradiated data obtained recently on various presently available graphite grades irradiated in the European Commission FP5, FP6 and FP7 RAPHAEL and ARCHER programmes are also included.

Gilsocarbon was a semi-isotropic graphite manufactured using spherical coke particles. The graphite grades irradiated in the European program illustrated in this chapter included both medium and fine grain grades as given in Table 4; however the names of the manufactures have been excluded for commercial reasons.

Grade	Coke	Grain size	Process
MG-1	Petroleum	Medium	Extrusion
SFG-1	Petroleum	Super-fine	Iso-moulding
MG-2	Pitch	Medium	Extrusion
FG-1	Petroleum	Fine	Iso-moulding
FG-2	Petroleum	Fine	Iso-moulding

Table 4 **Graphite grades irradiated in the EU Framework Programme discussed in this chapter**

Dimensional change

When irradiated at a temperature of interest to Generation IV systems, ~300^{o}C to ~1200^{o}C, semi-isotropic nuclear graphite first shrinks and then expands, with increasing fluence. The rate at which this process occurs is a function of both the irradiation fluence and temperature. This behaviour is illustrated with respect to Gilsocarbon graphite in Figure 7.

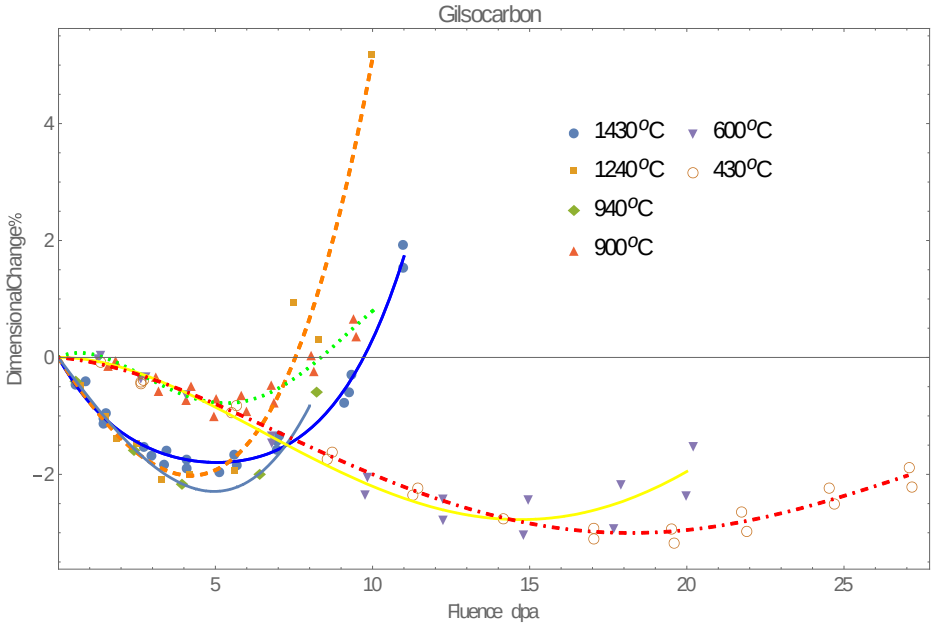

Figure 7 **Dimensional change in Gilsocarbon graphite irradiated between 430°C and 1430°C temperatures**

Gilsocarbon graphite is no longer available; however dimensional change of a medium grained (MG-2) and a fine grained (FG-1) graphite grades irradiated recently as part of the EU Raphael and Archer programmes are given in Figure 8 over a limited temperature range. It is interesting to note that despite the difference in grain shape and size, the dimensional change behaviour of these two graphite grades is similar to each other and to the behaviour of Gilsocarbon given in Figure 7.

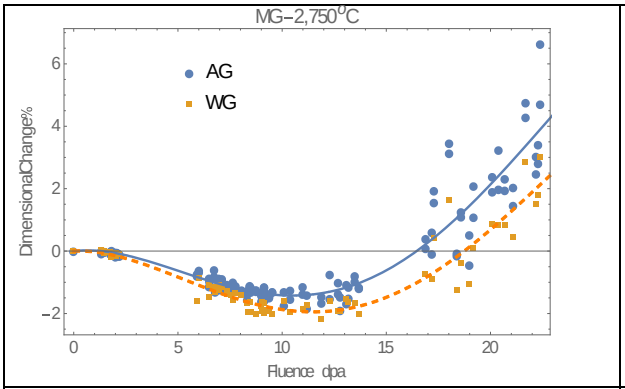

MG-2 Irradiated at 750°C

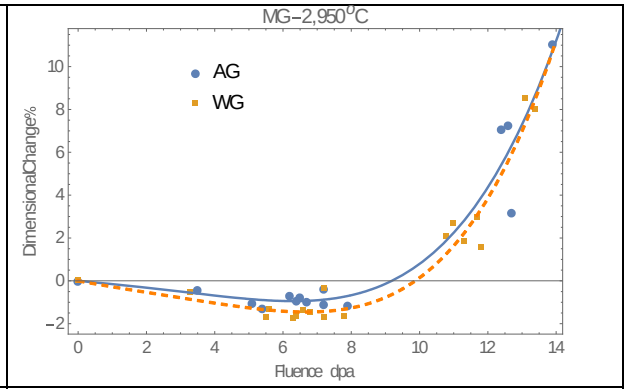

MG-2 Irradiated at 950°C

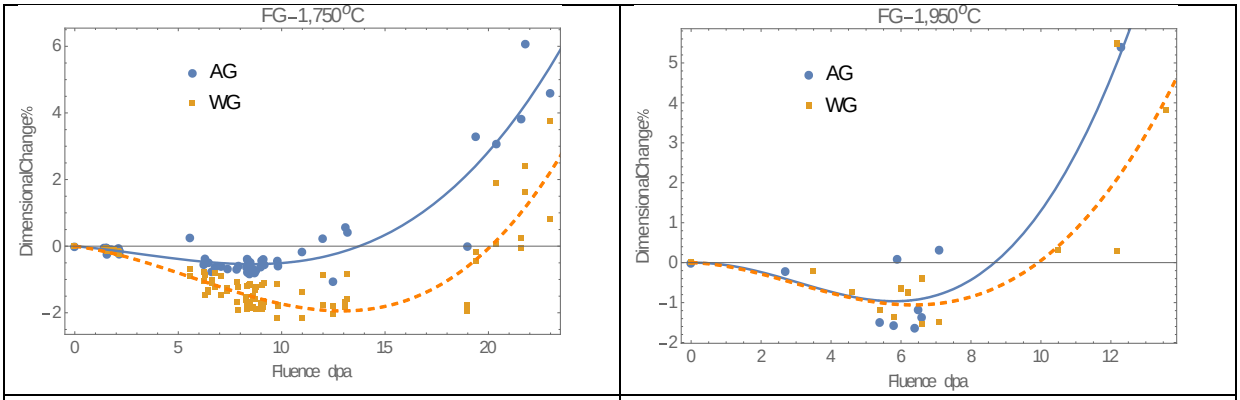

FG-1 irradiated at 750°C	FG-1 irradiated at 950°C

Figure 8 **Dimensional change in medium grained MG-2 and fine grained FG-1 nuclear graphite irradiated at 750°C and 950°C.**

The explanation for the shape of these dimensional change curves is related to the polycrystalline porous microstructure of nuclear graphite and the irradiation behaviour of the graphite crystallites as follows [10]:

- During graphite manufacture, due to thermal shrinkage during cooling from the graphitisation temperature, coupled with the large difference in the graphite crystal coefficient of thermal expansion CTE in the *c-axis*, ~27 x 10^{-6} K^{-1} (20-120°C), and *a-axis*, ~-1.5 x 10^{-6} K^{-1} (20-120°C), many nano to micro-sized cracks are formed which lie parallel to the graphitic basal planes, see Figure 3.
- Atomic displacement within the graphite crystal lattice leads to the formation of interstitial and vacancy loops causing the crystallites to swell in the *c*-axis and to shrink, at a slower rate, in the *a-axis*, see Figure 9.
- Initially the crystallite *c-axis* swelling can be accommodated by the many nano-and micro-cracks. Thus at the bulk component scale only the a-axis shrinkage is observed. However, as the *c-axis* nano-crack accommodation becomes exhausted, the *c-axis* swelling becomes dominant and significant bulk expansion takes place as shown in Figure 7 and Figure 8.

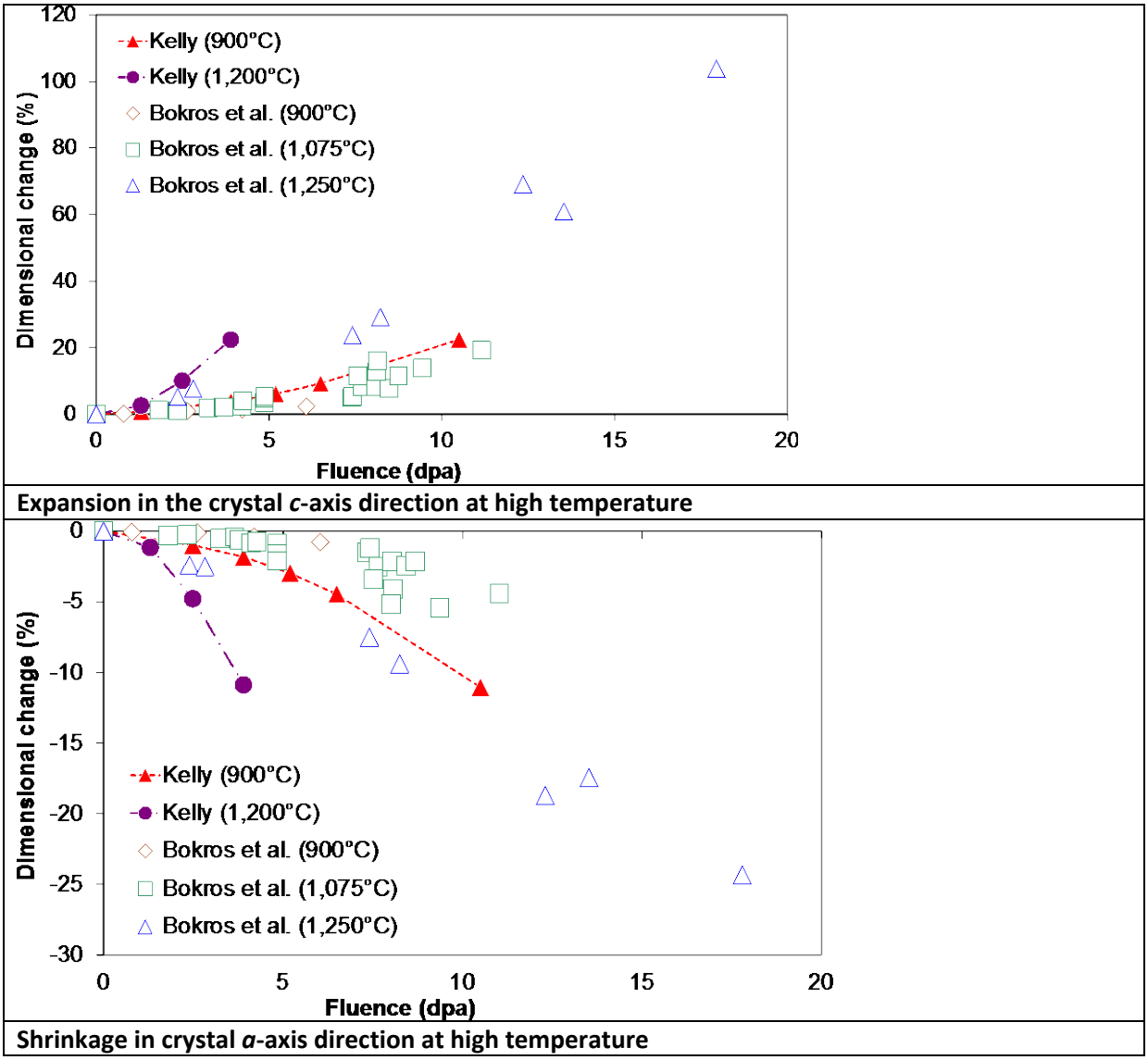

Figure 9 **Dimensional Changes in Highly Orientated Pyrolytic Graphite (HOPG) irradiated at high temperatures**

For use in stress analysis it is useful to fit curves to the data accounting for material variability and measurement uncertainty [17,18]. The form of the equation has to take account of not only the overall shrinkage and swelling behaviour but also a small region of initial swelling usually only observed at the lower temperatures, see Figure 8. Equation 3 is of a suitable form to fit the data in this chapter, but as with the other irradiated property/fluence relationships in this chapter the reader may choose alternative forms. The equations presented here are used for illustration only.

$$\frac{\Delta L}{L} = (1 - e^{-a\gamma})(b\gamma^3 + c\gamma^2 + d\gamma + e) \qquad 3$$

where, $\frac{\Delta L}{L}$ is linear dimensional change, γ is the fluence and, *a*, *b*, *c*, *d* and *e* are constants for

dimensional change. If data is available over a reasonable irradiation temperature range, some, or all, of these could be also functions of temperature [17].

Coefficient of thermal expansion

The change in the coefficient of thermal expansion (CTE) in irradiated Gilsocarbon graphite is given in Figure 10. Again, strong temperature dependence is clear; the changes in the CTE are more rapid with higher irradiation temperatures. The CTE data given in Figure 10 and also in Figure 11 are over the temperature range of 20-120°C, this can be converted to another temperature range by using the methodology described by Tsang and Marsden [19].

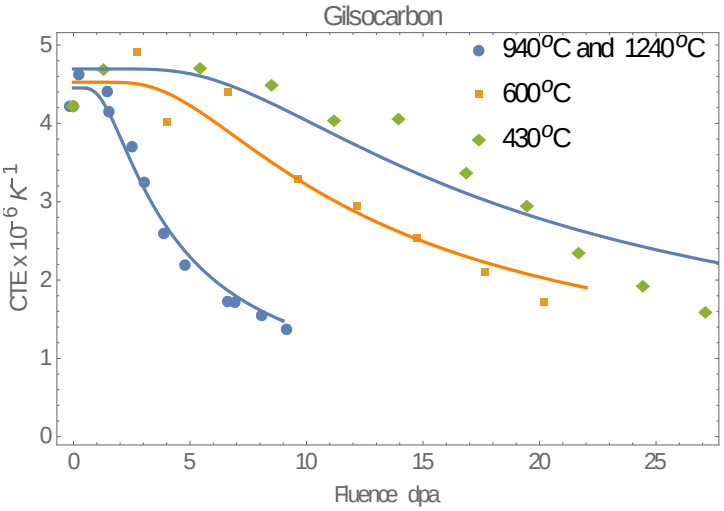

Figure 10 **Change in CTE in Gilsocarbon graphite irradiated at different temperatures**

The change in CTE in MG-2 and FG-1 medium and fine grade graphite irradiated as part of the EU Raphael and Archer programmes are given in Figure 11, again the CTE irradiation behaviour of these two grades is similar to that of Gilsocarbon.

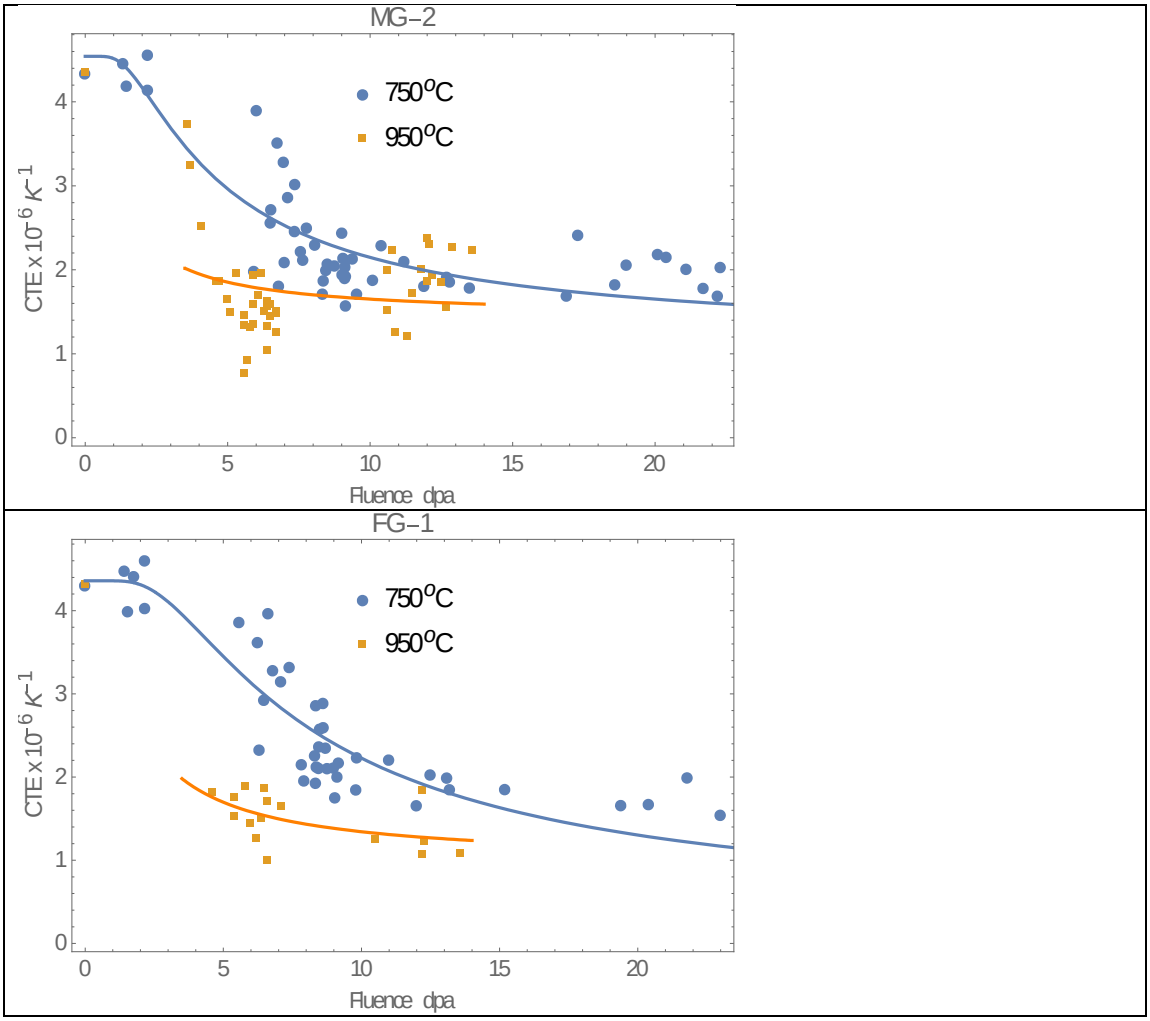

Figure 11 **Change in CTE in medium grained MG-2 and fine grained FG-1 nuclear graphite irradiated at 750°C and 950°C.**

In all cases there appears to be firstly a slight increase in the CTE followed by a steady fall before saturating at a value of about half the original virgin CTE. This behaviour is not simple to easily understand. The unirradiated crystal CTE measured over the range 20-120°C is 27.5 x 10^{-6} K^{-1} and -1.5 x 10^{-6} K^{-1} in the *c-axis* and *a*-axis, respectively. MTR measurement of crystal CTE in samples irradiated in the temperature range of interest to HTRs are invariant to irradiation fluence [20], so one may expect the bulk CTE not to change with increasing fluence, however it does. Therefore, the change in CTE shown in Figure 10 and Figure 11 is probably related to changes in the graphite structure at the micrometre scale as dimensional changes modify the porosity. Furthermore, the closure of nano- and micro-cracks which is attributed to dimensional change behaviour would be expected to increase CTE not reduce it. There is certainly scope for more microstructural/property related research in this area.

Equation 4 is a suitable fit to the CTE data presented in this section.

$$\alpha = aTanh((\gamma - b)/(c\gamma + d)) \qquad 4$$

Where, α is the irradiated CTE, Υ is the fluence and a, b, c and d are constants which may be temperature dependent. It may be necessary to supply 'a' as a boundary condition based on any initial rise is CTE.

Thermal conductivity

Irradiated nuclear graphite thermal conductivity data is usually presented as the reciprocal, which represents the thermal resistivity. The thermal resistivity is usually plotted as a function of fluence and irradiation temperature similar to other irradiated material properties. Thermal resistivity data for Gilsocarbon plotted as fractional change is given in Figure 12. Thermal resistivity initially increases rapidly to a slightly rising plateau before a secondary increase at high fluence.

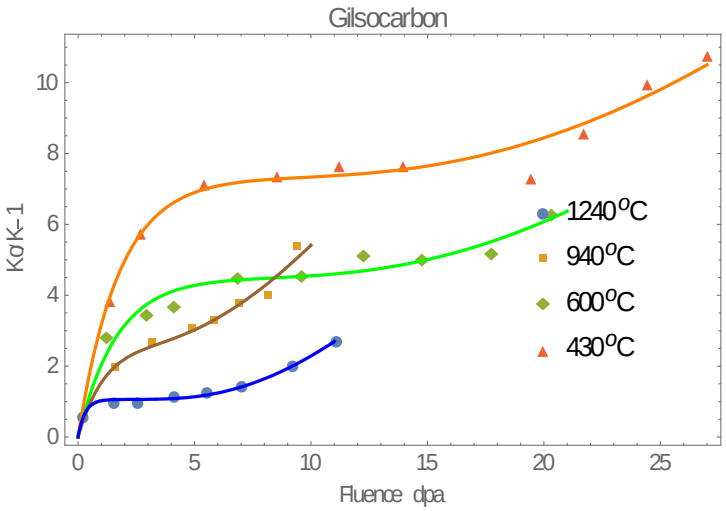

Figure 12 **Change in thermal resistivity of Gilsocarbon graphite irradiated at different temperatures**

The change in thermal resistivity with fluence in MG-2 and FG-1 at 750°C and 950°C, shown in Figure 13 as with the other properties, follows a similar trend to each other and to that of Gilsocarbon Graphite, as shown in Figure 12.

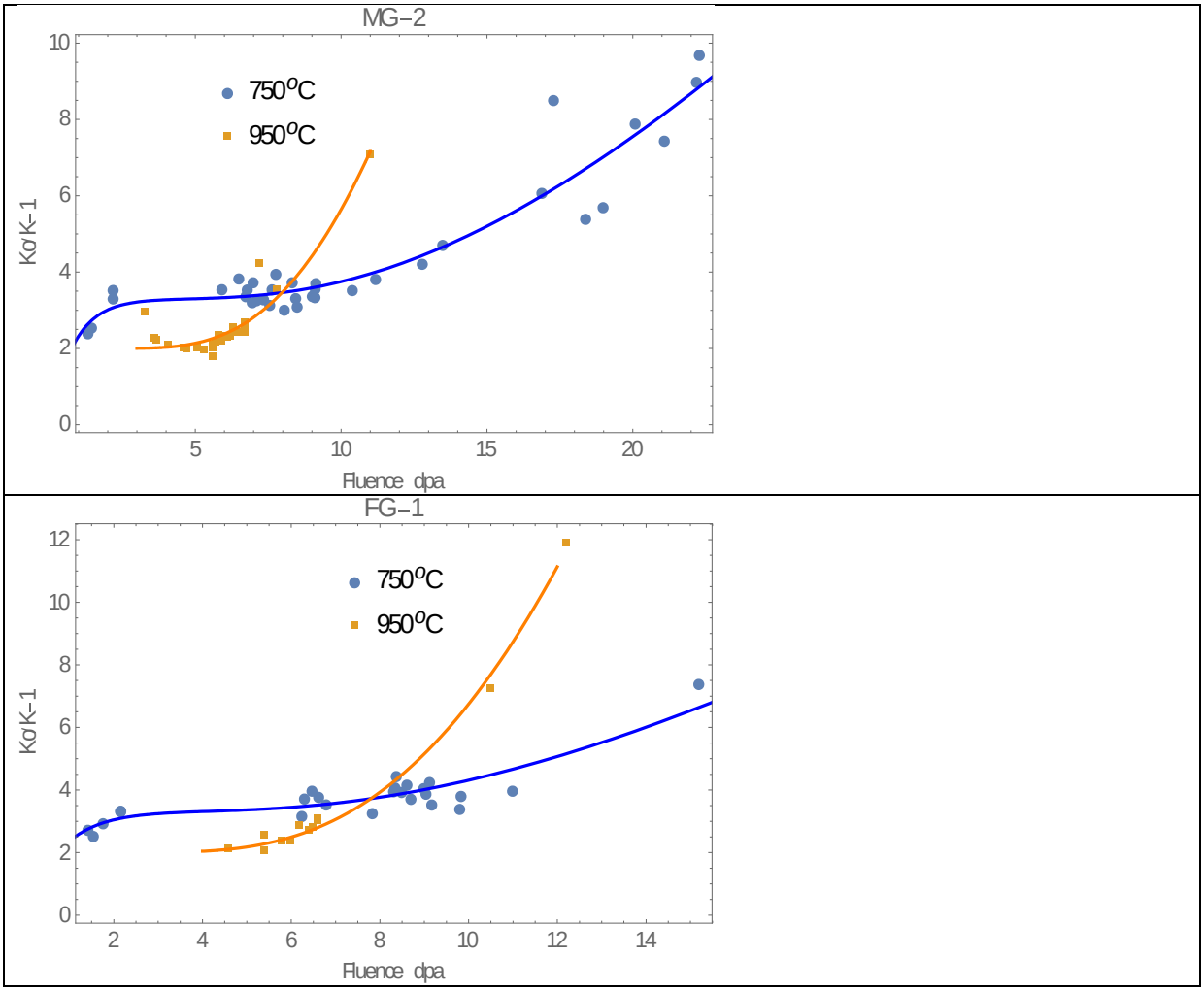

Figure 13 **Change in Thermal Resistivity in medium grained MG-2 and fine grained FG-1 nuclear graphite irradiated at 750°C and 950°C.**

The shape of the thermal resistivity curve is explained as follows. The thermal conductivity in graphite is mainly carried by lattice phonon vibrations and conduction is much higher along the basal plane than perpendicular to the basal plane [21]. Rising temperature leads to an increase in phonon-phonon scattering which reduces conductivity. Low amounts of fast neutron irradiation produce defects, interstitial and vacancies, which significantly disrupts the graphitic structure leading to an increase in phonon scattering thus reducing the conductance. This can explain the rapid increase in thermal resistivity which reduces in the medium fluence range. At high fluence the onset of inter-crystalline micro-cracking caused by large crystal dimensional change leads to a further deterioration in thermal conductivity. This latter phenomenon may be of particular importance when calculating heat transfer during thermal transients late in reactor life.

Equation 5 can be used to fit the initial and secondary rise in thermal resistivity data.

$$\frac{K_o}{K} - 1 = (1 - Exp[-a\gamma]) + Exp\left[-\frac{b}{\gamma}\right]\gamma \qquad 5$$

Where *K i*s the irradiated thermal conductivity, K_o is the unirradiated thermal conductivity, $\frac{K_o}{K} - 1$ is the fractional change in thermal resistivity, Υ is the fluence and *a* and *b* are constants which may be temperature dependent.

Young's modulus

The change in Young's modulus in Gilsocarbon graphite is given in Figure 14. With increasing fluence there is an initial rapid increase in modulus followed by a plateau region, which in some cases is not flat but slightly increases, followed by a rapid increase in modulus to a peak value before a steady but significant reduction. Again there is strong temperature dependence, the higher the irradiation temperature the more rapid the changes.

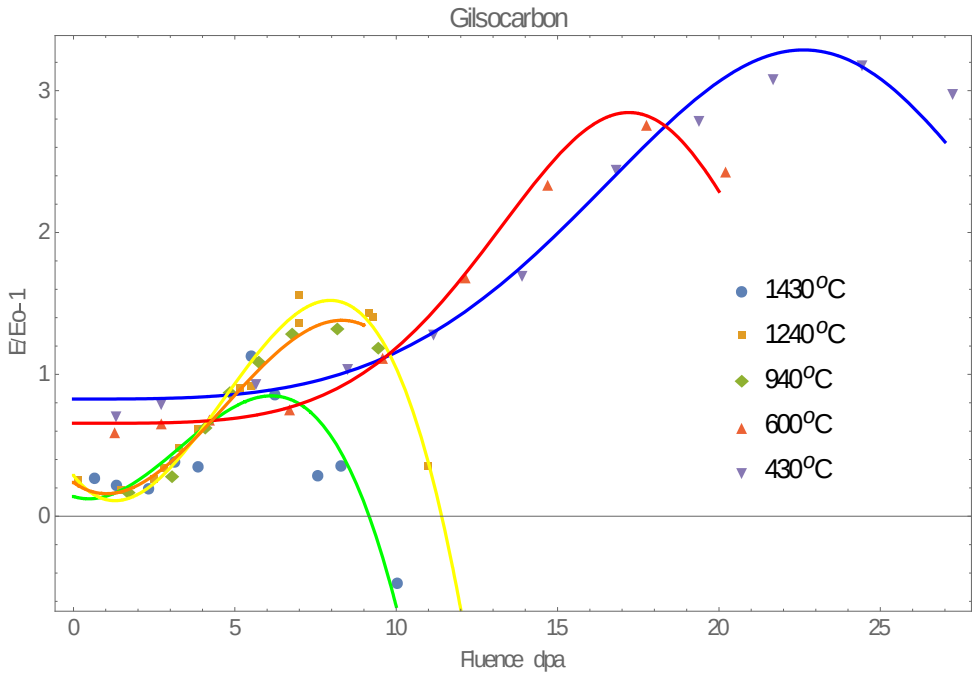

Figure 14 **Change in Young's modulus in Gilsocarbon graphite irradiated at different temperatures**

The data for the change in Young's modulus with fluence in MG-2 and FG-1 at 750°C and 950°C, as is the case with the other properties, follows a similar trend to that of Gilsocarbon Graphite, See Figure 15.

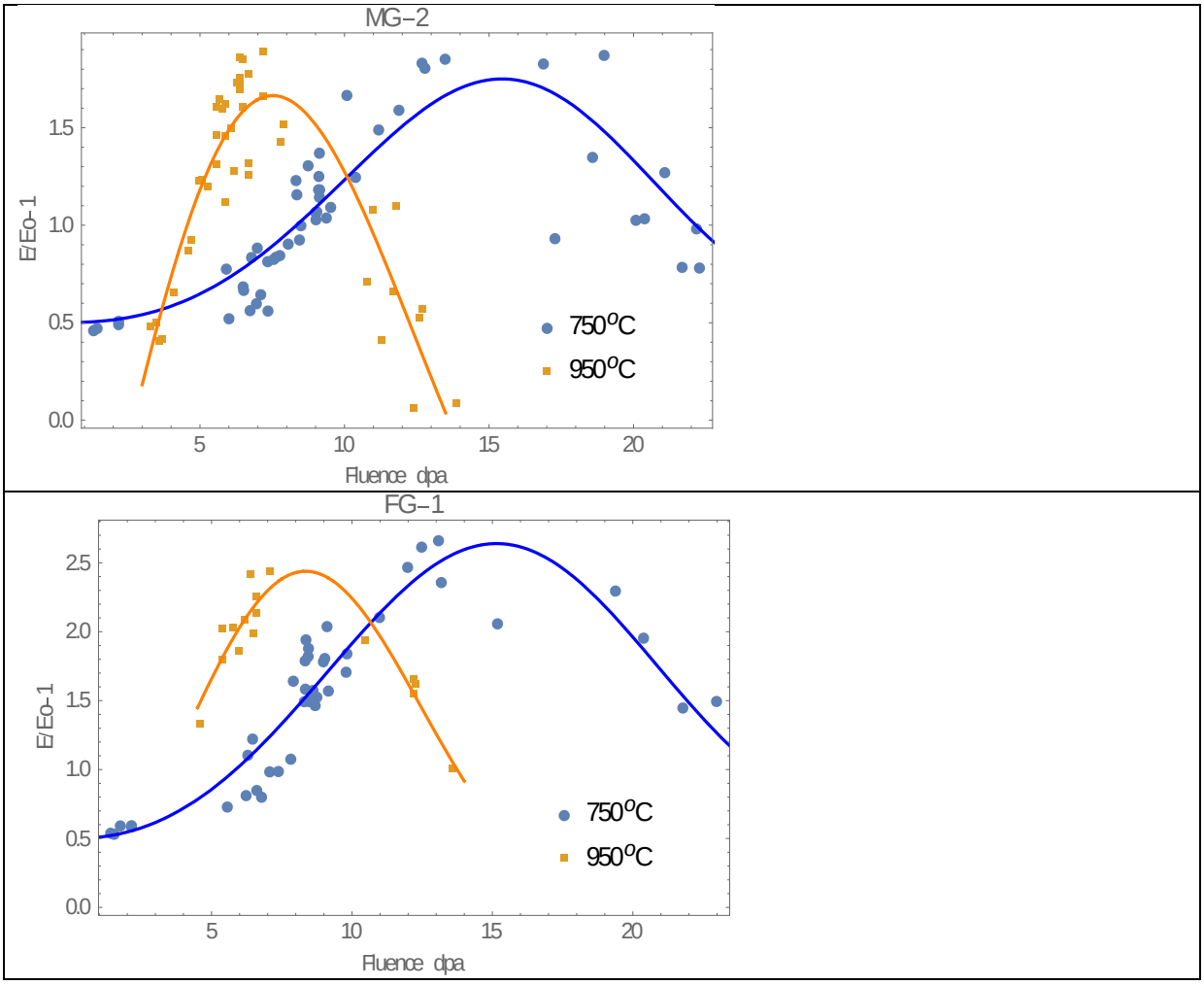

Figure 15 **Change in Young's modulus in medium grained MG-2 and fine grained FG-1 nuclear graphite irradiated at 750°C and 950°C.**

The mechanisms that govern this behaviour are attributed firstly to irradiation induced pinning of the crystallite basal planes, i.e. the crystallite C_{44} [22] shear modulus, leading to the initial rapid increase in the bulk modulus. The secondary increase in modulus is purported to be related to tightening of the microstructure due to large crystal dimensional change and reduction in porosity [23]. The final reduction in modulus is due to micro-cracking caused by the very large crystal changes at high fluence. If the graphite is irradiated through swelling into high volume change, significant cracking can occur and both modulus and strength decrease significantly, see Figure 16.

Elastic Poisson's ratio is usually taken as 0.2 [24]. It should be noted that it is usual to measure Young's modulus using a dynamic method (DYM). Therefore, when carrying out structural integrity assessments, this may require converting to a static value, see [25].

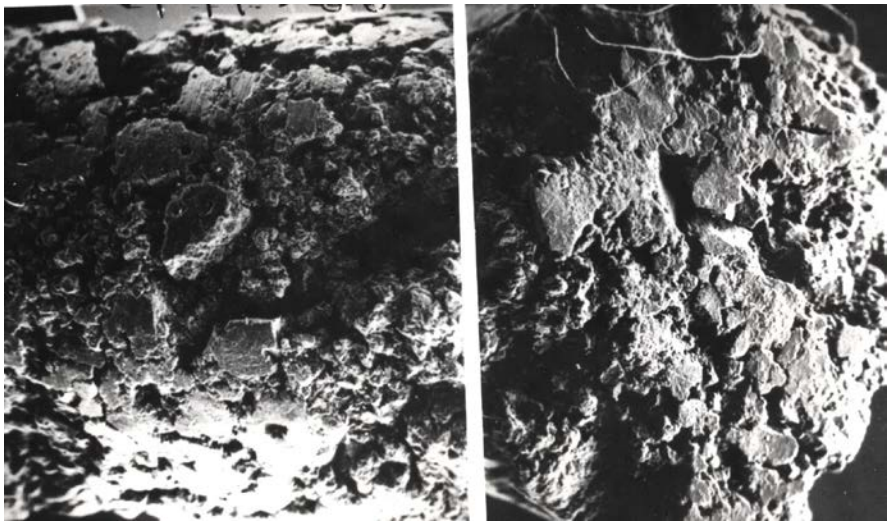

Figure 16 **SEM images of Gilsocarbon sample irradiated through into high volume change, 271 x 10^{20}** n/cm^2 EDND, Volume change 33%

The modulus data may be fitted to an equation of the form:

$$\frac{E}{E_o} - 1 = a + b\left(\frac{\gamma}{c}\right)^{(d-1)}\left(Exp\left[-\left(\frac{\gamma}{c}\right)^{d}\right]\right) \quad 6$$

Where $\frac{E}{E_o} - 1$ is the fractional change in Young's modulus E, E_O is the virgin Young's modulus, γ is the fluence and a, b, c and d are constants which may be temperature dependent. For Gilsocarbon the graphite ratio of static to dynamic Young's modulus E_s/E_{DYM} is usually taken as 0.84 and 0.92 for unirradiated and irradiated graphite, respectively [10].

Strength

A comprehensive study of the strength of irradiated nuclear graphite was carried out as part of the European Raphael and Archer projects. Failure strength was obtained using disc compression tests for both unirradiated and irradiated samples of medium grained, fine grained and supper fine grained nuclear graphite. The results are shown in Figure 17. Hoop strength is plotted in the figures; as this may be related to flexural strength using the methodology given by Berre, see chapter 8 of reference [26]. It should be noted that the curves are not well defined between zero and ~7dpa, however it can be seen that the general shape of the curves follows that of Young's modulus curves. As with Young's modulus the mechanism that causes this increase in strength can be understood by three stages: i) initial pinning of crystal basal dislocations giving rise to a rapid increase in strength, ii) then with increasing fluence tightening of the microstructure due to crystal dimensional changes further increasing strength until a maximum point is reached, iii) finally the crystal dimensional changes become so large that significant micro-cracking occurs and strength decreases, see Figure 16.

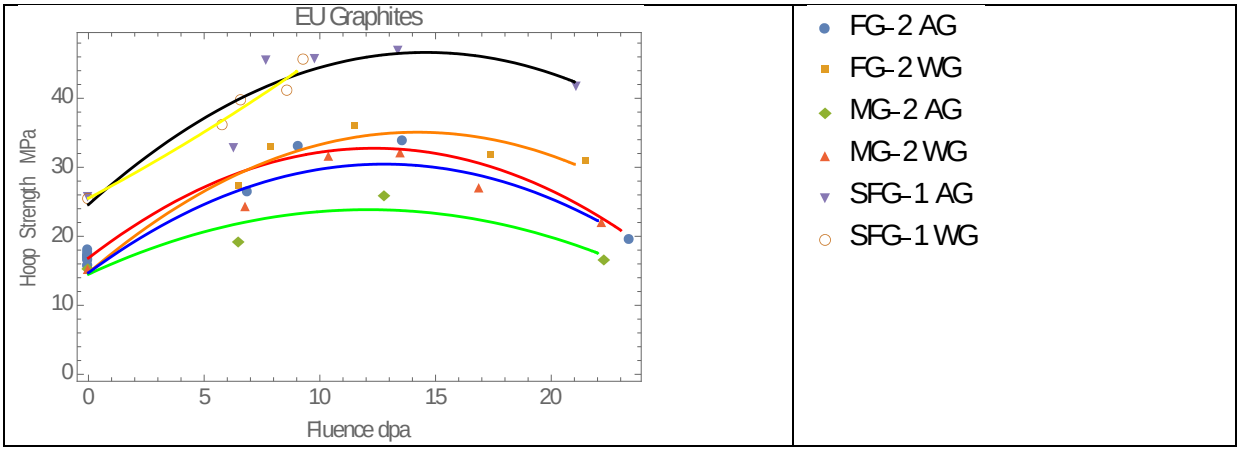

Figure 17 Tensile (Hoop strength) in medium, fine and supper fine graphite

Losty et al. [27] found that if the work to fracture could be assumed to not change by irradiation, the strength of Pile graphite was directly proportional to the square root of the modulus based on irradiation data and Griffith's criteria [28]; i.e. the critical failure stress, σ_f, at fracture for a body containing a sharp crack of length '2*c*' can be expressed as:

$$\sigma_f \approx \left(\frac{2E\gamma}{\pi c}\right)^{1/2} \qquad 7$$

where *E* is Young's modulus and γ is the effective surface energy per unit area, which is assumed to be invariant to irradiation fluence. This leads to the following relationship:

$$\frac{\sigma}{\sigma_o} = \sqrt{\frac{E}{E_o}} \qquad 8$$

where σ/σ_o is the ratio of irradiated to unirradiated strength and E/E_o is the ratio of irradiated to unirradiated Young's modulus. However, this relationship has been questioned by Marsden et al. [29] who reviewed strength and modulus data on a wide range of graphite grades. To test this hypothesis for the EU graphite grades, the modulus and strength data are plotted in Figure 18. The solid line is fitted to the data giving $\sigma/\sigma_o = 1.12(E/E_o)^{0.49}$ with an R^2 value of 0.97 which appears to agree reasonably with the square root approximation of Losty et al. [30], although there is a considerable amount of scatter in the data.

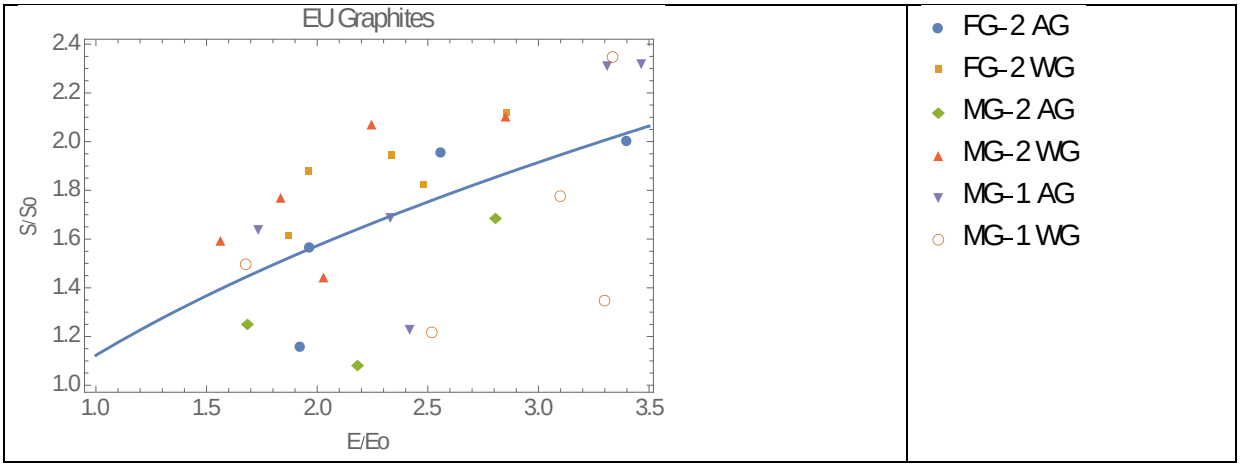

Figure 18 **Relationship between Young's modulus and strength in medium and fine grained graphite**

Irradiation creep

Very high temperatures ~2400°C are required to produce any significant thermal creep in graphite. However, in the presence of fast neutron irradiation, graphite will creep significantly at reactor operating temperature. This can be shown experimentally by irradiating small samples in a Material Test Reactor (MTR) under load and comparing their behaviour with an unloaded "control" specimen [31]. Compressive loading causes the dimensional change shrinkage to increase. Tensile loading reduces the amount of dimensional change shrinkage. Subtracting the control specimen data from the loaded specimen data and plotting the mathematical modulus of both the compression and tensile results gives the "irradiation creep curves" shown in Figure 19 for graphite grades intended for use in USA and German HTRs.

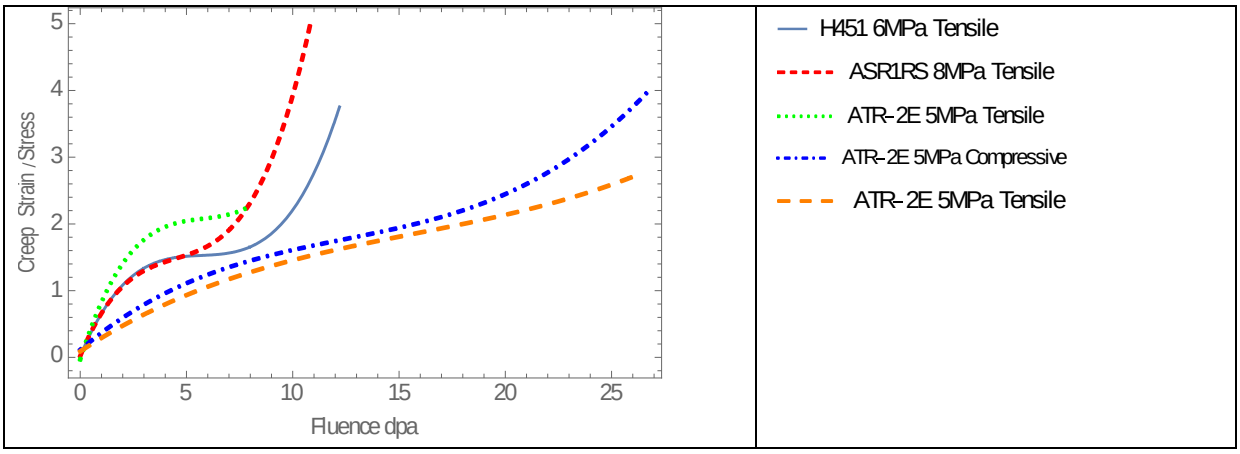

Figure 19 **Curves fitted to high temperature creep data, samples irradiated in HFR Petten [32]**

Early irradiation creep MTR data in the temperature range ~300-600°C to a fluence of ~60 x 10^{20} n/cm^2 EDND obtained by the UKAEA [31] from graphite samples machined from the extremely anisotropic Magnox PGA and semi-isotropic AGR Gilsocarbon graphite indicted that, in this temperature and fluence range, there was a short period of recoverable primary creep followed by a linear secondary creep phase. In addition, the tensile and compressive creep data for these two very different nuclear graphite grades, when plotted as strain units defined by $esu = \frac{\varepsilon_{cr} E_o}{\sigma}$ where ε_{cr} is the creep strain, σ is the applied stress and E_o is the unirradiated elastic modulus, fitted Equation 9, see Figure 20. In the case of equation 9 the fluence γ is in units of n/cm^2 x 10^{20} EDND. Poisson's Ratio for creep is normally taken as being the same as the elastic value of 0.2, although there is some evidence that it increases with creep strain [33].

$$\varepsilon_{cr} = \frac{\sigma}{E_o}\left(1 - exp(-4\gamma)\right) + 0.23\frac{\sigma}{E_o}\gamma \qquad 9$$

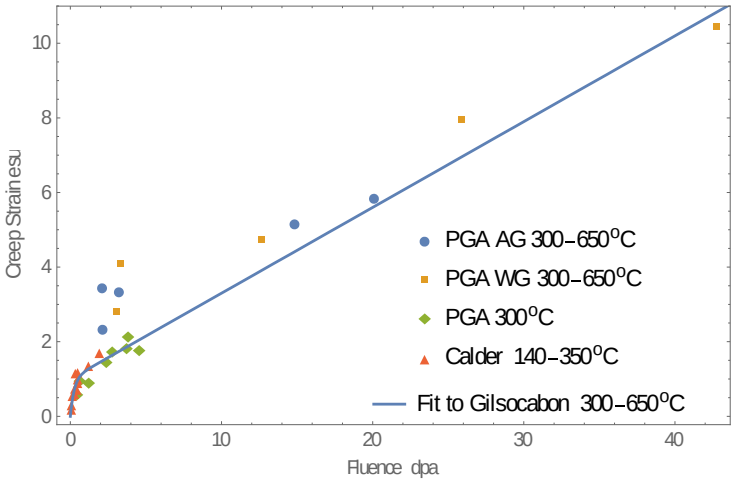

Figure 20 **UKAEA creep data for anisotropic PGA and isotropic Gilsocarbon under tension and compression [31]**

To try to account for the effect of radiolytic oxidation in the Magnox and AGR, further, but limited higher dose creep data was obtained on pre-irradiated inert and oxidised samples. This led to the modification of equation 9 by instead of normalising the data to the unirradiated modulus, E_o, a modified creep modulus, E_c, was used which is defined as:

$$E_c = E_o SW \qquad 10$$

Where S is the irradiation induced change in modulus, $[E/E_O]$, divided by the initial rise in modulus (referred to as the pinning term), $[E/E_O]_P$, as shown in Equation 11. W is a weight loss term.

$$S = \frac{\left[E/E_o\right]}{\left[E/E_o\right]_P} \qquad 11$$

Taking into account the change in creep rate with temperature and accounting for variation in stress, Equation 9 then becomes:

$$\varepsilon_{cr} = \alpha(T)exp(-b\gamma)\int_0^{\gamma}\frac{\sigma}{E_c}exp(b\gamma')d\gamma' + \beta(T)\int_0^{\gamma}\frac{\sigma}{E_c}d\gamma' \qquad 12$$

Where the parameters $\alpha(T)$ and $\beta(T)$ are temperature dependant and "*b*" is a constant usually taken as 4. $\alpha(T)$ is the primary creep coefficient and is usually taken as unity while the parameter $\beta(T)$ is the secondary creep coefficient that can be obtained from a selection of Russian and US data see Figure 21. To justify the use of this equation, the UKAEA [31,34] developed a "pining-un-pining" model which attributes irradiation creep mechanism to basal plane slip [35].

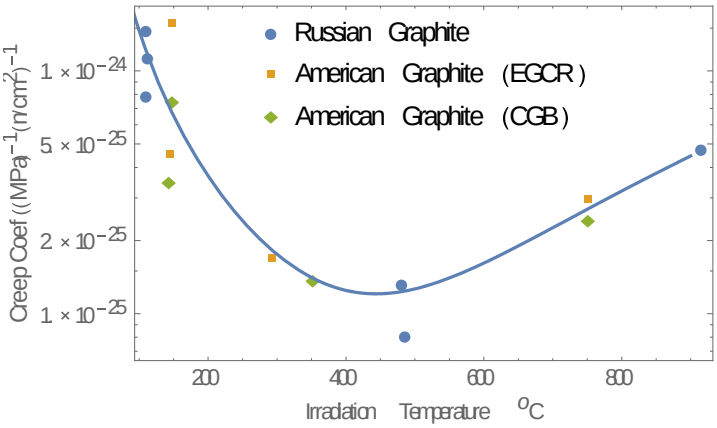

Figure 21 **Creep Coefficient as a function of temperature**

As part of the German and US HTR programmes a significant amount of high fluence, high temperature graphite irradiated data was produced as shown in Figure 19, but the accumulation of this data coincided with the abandonment of the German HTR programme and the data was not thoroughly written up and analysed.

From Figure 19 there appears to be a significant tertiary creep rate at high fluence and a difference between compressive and tensile creep rates. Furthermore, Equation 12 does not satisfactorily reconcile with all the curves given in Figure 19.

Another irradiation creep relationship proposed by Kennedy et al. [36] is capable of giving a good fit to the data:

$$\varepsilon_{cr(Secondary)} = K\left(\frac{\sigma}{E_o}\right) \qquad 13$$

where

$$K = K'\left[1 - \mu\frac{\Delta V/V_o}{\left(\Delta V/V_o\right)_m}\right] \quad 14$$

where K' is the creep coefficient which is temperature dependent, $\Delta V/V_o$ is the volumetric dimensional change and $\left(\Delta V/V_o\right)_m$ is the minimum volumetric dimensional change. μ is a constant that can be varied to enable a good fit to be obtained. This methodology uses the volumetric dimensional change as a surrogate for the structural changes influencing the creep rate which are driven by the dimensional change. The method, like the UKAEA theory, assumes that there is some underlying basal plane slip mechanism. Primary creep can be included using the same transient term as given by Equation 12.

Further complication arose from data showing that when previously irradiation crept graphite samples were irradiated for a significant time with the load removed the amount of recovery was far greater than one elastic deflection [37]. This led to the development of a much more complex model [38].

Recently an IAEA coordinated research programme (CRP) was established in order to review the present position. The findings of this committee will shortly be published as an IAEA technical document (TecDoc). One important finding of the review is that the quality of the temperature control in the Petten irradiation creep experiments is questionable. The large dimensional changes in the specimens at high fluence will have closed the gaps between the specimens and the specimen holders causing the specimens to run hotter than intended; this may go some way to explain some, if not all, of the tertiary creep shown in Figure 19.

There are various other irradiation creep models of varying complexity in the literature [38, 39]. However, without a more extensive and well validated set of data covering a range of loading (tensile and compressive), fluence, unloading, direct and lateral dimensional changes, all the present models must be considered to be speculative. For present reactor design, as long as stress raisers are avoided Equations 12 and 14 are probably suitable.

Influence of strain on the coefficient of thermal expansion

When conducting irradiation creep MTR experiments [40], it was found by the UKAEA that in the crept specimens the CTE differed from that of the control specimens, i.e. the CTE was greater in the compressive samples and less in the tensile specimens. At first it was considered that there was a direct relationship between creep strain and CTE. However, later it was shown that direct stress in unirradiated graphite could also change the CTE [41] in a similar manner, and when the two sets of data were plotted alongside each other a similar relationship was obtained, see Figure 22. Other authors [39] have obtained similar results in other graphite grades.

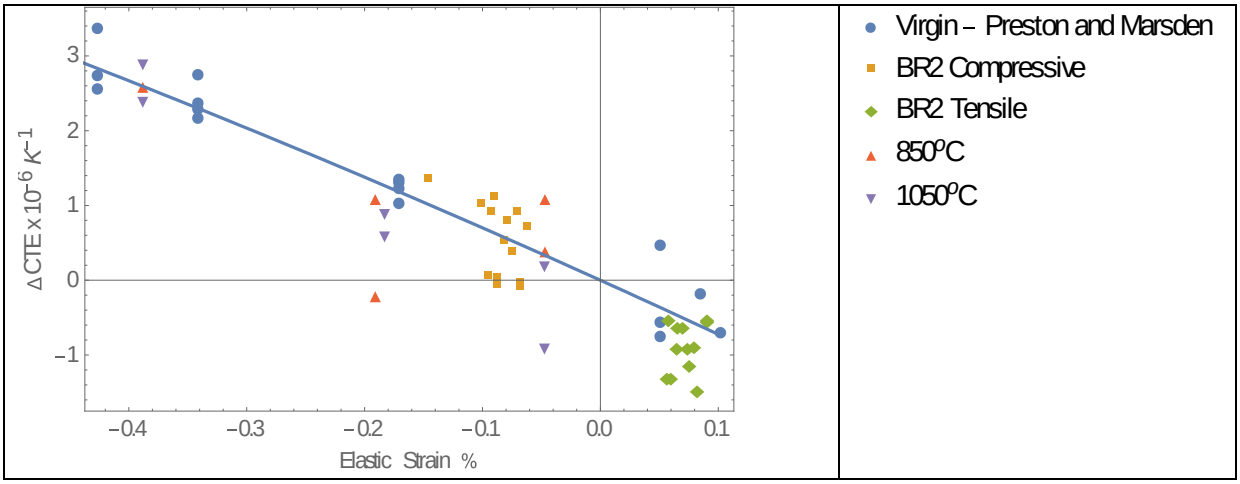

Figure 22 **Change in CTE as a function of elastic strain in crept irradiated and stressed virgin Gilsocarbon graphite.**

This finding has implications for graphite component stress analysis, because the CTE is not only a function of irradiation fluence and temperature but is also a function of strain.

In recent years it was decided to define CTE as a function of primary creep strain [38]. However, primary creep strain and elastic strain are similar in magnitude, i.e. approximately one elastic deflection. The experiments on virgin Gilsocarbon also determined a lateral effect of change in CTE with strain; however '0.2 x the direct change' is often used in stress analysis. Care must be taken in regions of high tensile stress as the data in the tensile region of Figure 22 is scattered with no well-defined trend and in addition the tensile range of the data is limited, so in the region of sharp corners or other stress raisers the limit of the data may be exceeded.

Component structural integrity

Structural integrity calculations for nuclear components are usually carried out using conventional finite element (FE) stress analysis programmes with the inclusion of a nuclear graphite "user material" subroutine [42,43].

The basic input required are:

1. *Spatial and time dependent field variables including*:
    a. Irradiation fluence history, provided from a reactor physics code
    b. Irradiation temperature history determined using:

i. a thermos-hydraulic code to calculate gas temperatures boundary conditions
ii. a reactor physics code to calculate component gamma and neutron heating
iii. a thermal finite element code to determine the temperature distributions. These calculations will also require graphite thermal conductivity as a function of fluence and temperature as well as graphite density.

c. Component external loading history may be required in some cases, again probably calculated using a finite element stress analysis code

2. The virgin graphite material properties
   a. Young's modulus
   b. Poisson's ratio
   c. Coefficient of thermal expansion

3. *Material property data as a function of irradiation fluence and temperature*
   a. Dimensional change
   b. Coefficient of thermal expansion
   c. Young's modulus
   d. Poisson's ratio
4. An irradiation creep relationship as a function of fluence, temperature and stress
5. The change in the coefficient of thermal expansion as a function of strain
6. Account must be taken of the change in virgin and irradiated graphite CTE, Young's modulus and strength with temperature.

The spatial and time dependent field variables and materials data are either provided as numeric tables of numbers or by equations fitted to the raw experimental points.

The relationship between the incremental stress, $\Delta\sigma$, and the incremental elastic strain, $\Delta\varepsilon_E$, is defined by:

$$\{\Delta\sigma\} \cong [D]\{\Delta\varepsilon_E\} \qquad 15$$

Where [*D*] is the two or three dimensional elastic matrix relating stresses to strains [44].

As a consequence of the irradiation induced property changes a number of strains will develop within the component which are related to the elastic strain as follows:

$$\{\varepsilon_E\} = \{\varepsilon_{TOT}\} - \{\varepsilon_{pc}\} - \{\varepsilon_{sc}\} - \{\varepsilon_{\gamma}\} - \{\varepsilon_{th}\} - \{\varepsilon_{\text{int}}\} \qquad 16$$

Where:

- ε_{ToT} is the total strain
- ε_{pc} and ε_{sc} are the primary and secondary creep strains, defined by Equation 12, or by a similar relationship
- ε_{γ} is the strain due to dimensional changes
- ε_{th} is the thermally induced strain due to component temperature gradients

- ε_{int} results from the additional changes in CTE due to elastic/primary-creep strain

Assuming a central difference operator for stress $\{\sigma\} = \{\sigma_o\} + \left\{\frac{\Delta\sigma}{2}\right\}$, the increment in stress can then be defined as:

$$\{\Delta\sigma\} = [D](\{\Delta\varepsilon_{TOT}\} - \{\Delta\varepsilon_{\gamma}\} - \{\Delta\varepsilon_{th}\} - \{\Delta\varepsilon_{\text{int}}\}) \quad 17$$
$$- [D][D_c]\{\sigma_o\}(\alpha+\beta)\Delta\gamma - [D][D_c]\left\{\frac{\Delta\sigma}{2}\right\}(\alpha+\beta)\Delta\gamma$$

Where $[D_c]$ is the creep stress/strain relationship matrix.

Many modern commercial finite element codes have the facility to use and adapt Equation 17 to provide the material Jacobian matrix, $\partial\Delta\sigma/\partial\Delta\varepsilon$, for the irradiated graphite constitutive model to the FE code.

Figure 23a shows a model from the finite element analysis of an HTR reflector block. The mesh shows half the block with two holes which are the channels for the control rods and the inlet gas passage to the upper premium. Figure 23b shows the fast neutron fluence which varies from 100 × 10^{20} n/cm^2 EDND on the inside to 1 × 10^{20} n/cm^2 EDND on the outside. The irradiation temperature is 500°C on the inside and 200°C on the outside. The results in Figure 23 are at an irradiation time of 30 full power years.

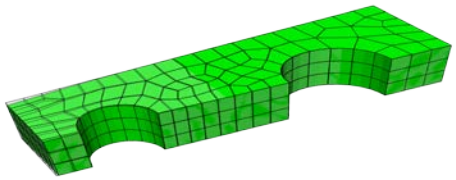

a) Finite element mesh, showing deformed shape, after irradiation of Pebble Bed HTR reflector block

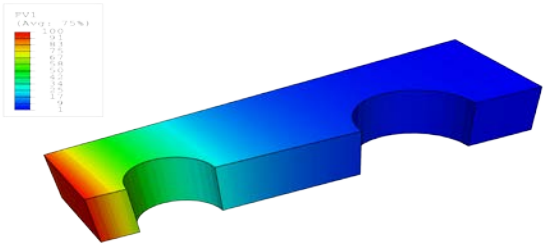

b) Contour plot of fast neutron fluence. The inside (red) is 100 × 10^{20} n/cm^2 EDND and the outside (deep blue) 1 × 10^{20} n/cm^2 EDND

Figure 23 **Finite element analysis of HTR Pebble Bed reflector block**

Thermal oxidation in fault conditions

Nuclear graphite gas reactions are well documented [2,5,27,45–53]; kinetically the rates are very slow at temperatures below 400 °C. The operating temperatures of a HRT or MSR are suitability elevated that if any oxidising gaseous species where to enter the core under fault conditions, such as steam or O_2 ingress via a burst pipe, then high rates of graphite oxidation could readily occur. This behaviour has been examined using various different oxidising gas species, different types of graphite and different temperatures focusing on reactive gas species of greatest historic interest

such as oxygen (O_2), carbon dioxide (CO_2) and water vapour (H_2O) as well as the primary gaseous products of the arising graphite oxidation reactions: carbon monoxide (CO) and hydrogen (H_2). There are a number of relevant primary and secondary reactions that lead to carbon gasification, as described by Walker's review paper [45] and others [2,5,27,45–53]. These include reaction of carbon with oxygen, steam, carbon dioxide and hydrogen and are shown in Table 5 with their corresponding heats of reaction at 18°C and 1 atmospheric pressure.

Table 5 **Graphite gas reactions and enthalpy values**

Carbon-Oxygen Reactions	**Heat of Formation (ΔH, kJ/mol)**
$C(s) + O_2(g) \leftrightarrow CO_2(g)$	ΔH = -393.4
$C(s) + \frac{1}{2}O_2(g) \leftrightarrow CO(g)$	ΔH = -111.4
$CO(g) + \frac{1}{2}O_2(g) \leftrightarrow CO_2(g)$	ΔH =-282.0
$C(s) + H_2O(g) \leftrightarrow CO(g) + H_2(g)$	ΔH =135.6.0
$C(s) + 2H_2(g) \leftrightarrow CH_4(g)$	ΔH =-88.6

All but one of these reactions are exothermic, the first has a heat of reaction of 94 kcals/mole and the second two combine to the same total leading to the same eventual product. If there is an excess of oxygen, then mainly CO_2 will be produced with increasing CO amounts for an oxygen-depleted condition. Once started, the reaction can easily become self-sustaining. The reaction between air, containing approximately 21% oxygen, and graphite only becomes significant at temperatures of the order of 400°C [54].

The oxidation of graphite at different temperatures is controlled by three mechanisms (or modes): the chemical mechanism at temperatures below 500 °C, the in-pore diffusion-controlled mechanism at temperatures between 500 and 900 °C and the boundary layer controlled mechanism at temperatures over 900 °C. A graphical representation of how these differ in terms of reaction rate and oxygen concentration into the graphite bulk is illustrated in Figure 24.

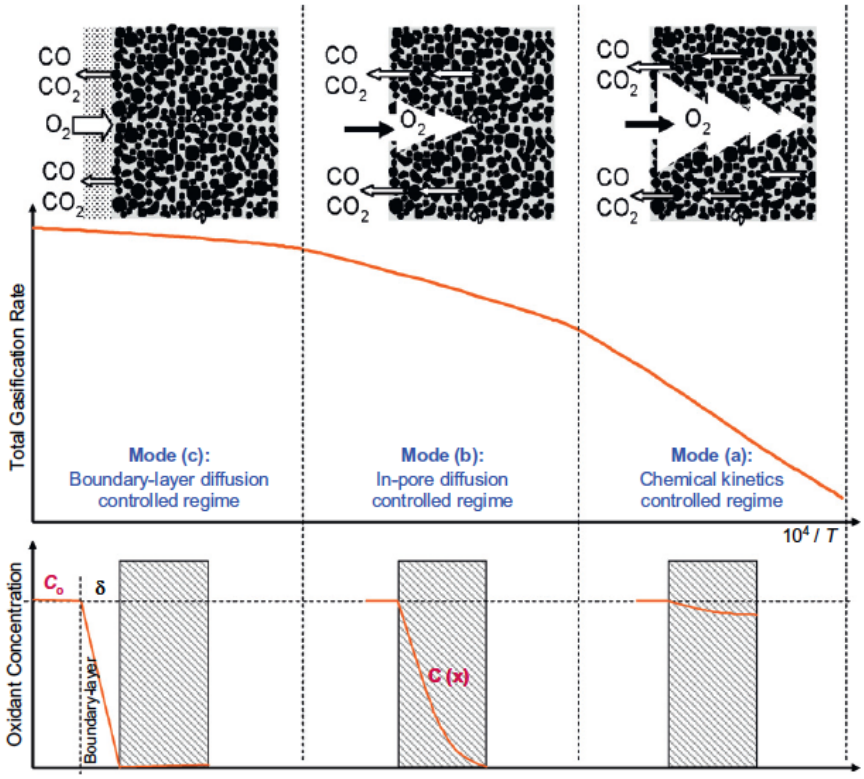

Figure 24 **Graphite oxidation modes of temperature regions and associated oxygen concentration [55]**

Mode A – Chemical Regime: The first regime is the lowest temperature regime in which the reaction rate is essentially determined by the rate of the chemical reaction, whereby the distribution of oxygen throughout the open porosity can be considered as constant, and so reaction occurs at all 'open' surfaces throughout the bulk of the body. The graphite geometry remains largely unaffected in this regime as the majority of surface area is found in internal porosity. At these lower temperatures, the transport of oxidant into the structure and reaction products out of the structure is unconstrained and does not affect the reaction rate.

Mode B – In-pore Diffusion Regime: The second regime can be considered an intermediate regime between Modes A and B, where in-pore diffusion becomes more restrictive with increasing temperature. This occurs because at elevated temperatures the chemical reaction occurs more quickly than in Mode A, such that the rate at which oxygen can be transported to the internal pore surface and the rate at which the products can diffuse back out of the graphite are slow enough to inhibit the natural intrinsic rate of reaction. This can also occur in a material with a particularly restrictive structure.

One of the consequences of this is the development of a concentration gradient of reacting gases through the bulk of the graphite. The outer surfaces, those closer to the external gas flow, undergo preferential oxidation, as less oxidant is able to reach the internal surfaces furthest from the gas flow.

Mode C – Surface Boundary Layer Controlled Regime (>900 ^{o}C): The third regime applies to all temperatures above those applicable for Mode B. In this regime, which can be otherwise known as

the ‘mass transfer’ regime, the temperatures are elevated high enough, and the reactivity of the graphite increased, that the majority of the oxidant is consumed at the surface of the graphite without any penetration to the internal porosity. A boundary layer forms at the surface of the graphite, and it is the mass diffusion through this layer that limits the oxidation process; oxidants are restricted from accessing the graphite surface, and to some extent reaction products restricted from leaving, and so it is in this regime that the external geometry of the graphite will be most affected.

Whilst new grades of nuclear-grade graphite have excellent chemical, structural and neutronic properties for reactor use, they are known to oxidise in air at temperatures above 723 K [56]. Below this temperature the microstructure matrix and filler is not susceptible to oxidation. The concern with air oxidation is essentially twofold: (1) the chronic oxidation during normal operation by oxidizing impurities circulating in the helium coolant and (2) severe oxidation caused by an air ingress accident. During normal operation of an HTR, oxidising impurities carried by the circulating helium coolant in the primary reactor system can gradually oxidise reflector and fuel element components constructed of graphite [53,56,57]. A severe accident such as an air or water ingress accident would cause the graphite material to be oxidized by air or water. In the failed fuel element, gaseous and volatile fission products can be released. Thus, the integrity of the graphite structure may be forfeited due to enhanced oxidation [1,55,56,58–60].

Dealing with irradiated graphite waste

When designing a modern graphite moderated reactor it is important to choose very pure graphite, not only from a neutronic point of view but also to ensure the graphite irradiated waste does not contain any elements that will lead to high isotopic activity such as of cobalt, or long lived isotopes such as ^{36}Cl or ^{14}C which may arise from ^{35}Cl or ^{14}N. However, in the past in some cases reactor designers have not paid as much attention to purity in graphite selection as should have been done.

Graphite has been utilised in more than 100 nuclear power plants worldwide and in many research and plutonium-production reactors [8]. In the UK, once operations cease this will produce somewhere in the region of 100,000 tons of irradiated graphite waste [61,62]. The largest source of irradiated graphite originates from reactors’ moderator and reflector core materials. The majority of this graphite has been exposed to very high levels of neutron irradiation resulting in activation of impurity radionuclides. There are also other sources of irradiated graphite components, in addition to the moderator and reflector, such as Material Test Reactor (MTR) thermal columns, fuel channel sleeves, graphite plugs, outer circumferential fuel sleeves, graphite boats and side locating struts. Furthermore, the current move towards future Generation IV Very High Temperature Reactors (HTR) in some countries will result in significantly higher volumes of irradiated graphite requiring management in the future. This is predominately due to the high turnover of fuel pebbles, which are largely graphite/carbon in their composition. As the proposed Generation IV HTR and MSR designs employ graphite as a structural material, a viable and effective decommissioning plan must be demonstrated before approval is granted for such designs by the regulating bodies.

The current UK baseline strategy for reactor graphite is to dismantle reactor cores following a period of dormancy (typically 85 years) and package the graphite for disposal [61]. Disposal in a Geological Disposal Facility (GDF) is the planned end point for the packaged waste in England and Wales. The

Scottish Government Policy is that the long-term management of higher activity radioactive waste should be in near-surface facilities; and that those facilities should be located as near to the site where the waste is produced as possible/practicable. Developers will need to demonstrate how the facilities will be monitored and how waste packages, or waste, could be retrieved. All long-term waste management options will be subject to robust regulatory requirements.

To ensure the safe disposal of graphite, the activity associated with the radionuclides and the possible release of these radionuclides during decommissioning and disposal requires full assessment [62,63]. Graphite retains various radionuclides such as ^{3}H, ^{14}C and ^{36}Cl, as well as corrosion/activation products (^{57}Co, ^{60}Co; ^{54}Mn; ^{59}Ni; ^{63}Ni; ^{22}Na, etc.), fission products (^{134}Cs, ^{137}Cs; ^{90}Sr; ^{152}Eu, ^{144}Ce, etc.) and a small amount of uranium and transmutation elements (^{238}Pu, ^{239}Pu; ^{241}Am, ^{243}Am, etc.). Some of these radionuclides arise from the activation of impurities which were integral with the original graphite components, other radionuclides arise from other reactor materials, which have then been activated elsewhere in the core before being carried around the circuit in the coolant gas [64,65]. The foremost-activated material may be associated with the graphite component internal porosity surfaces, which may be transported deeper into the material via the complex porosity network. Immediately after shutdown ^{3}H is the predominant radionuclide in terms of activity, but with a half-life of 12.3 years this decays relatively quickly and ^{14}C eventually dominates. Both ^{14}C and ^{36}Cl have long half-lives, 5730 and 301,000 years respectively, and represent the radionuclides of concern for long-term waste management and disposal. Although there have been some recent efforts to determine the mechanism of ^{14}C generation [66], the understanding of speciation and location of ^{14}C which will vary with reactor type, graphite manufacturer, reactor operating history and location in the core is limited. The main routes for the generation of ^{14}C are via neutron activation of $^{13}C(n, \gamma / 0.0014$ barn), ^{14}N (n, p / 1.93 barn) and ^{17}O (n, α / 0.257 barn). Due to the fact that ^{17}O is only present in natural oxygen by 0.038 %, ^{14}C generation via ^{17}O is much less than by ^{13}C or by ^{14}N, in most nuclear graphite cases. As the activation cross section of nitrogen is about 1,400 times larger than that for ^{13}C, the same ^{14}C production is therefore already reached at a nitrogen concentration of about 8 ppm within graphite. It may thus be concluded that no two-reactor designs will result in irradiated graphite with similar properties when considered for disposal, since different operational histories will have a bearing on the radioisotope content and possibly on the location (and chemical form) of those radioisotopes. Large variations may also be apparent in the graphite arising from reactors of similar type (batch-to-batch variations in manufacturing, and longer-term trends in properties within the manufacturing process) as shown in the autoradiography results of irradiated graphite in Figure 25.

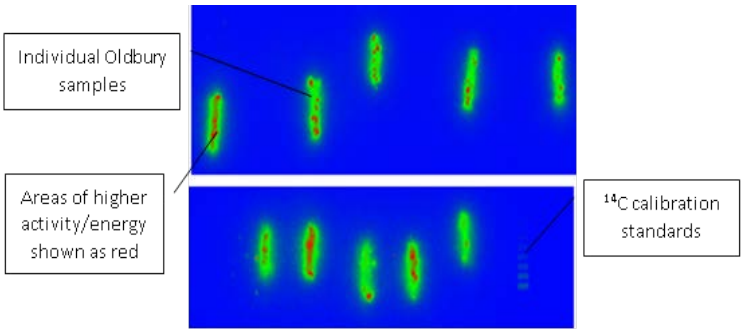

Figure 25 **Colour intensity image generated of Oldbury irradiated graphite samples using autoradiography showing radioactivity is distributed non-uniformly within a samples and the presence of high activity hot spots.**

This emphasises the need for sample characterisation where graphite is to be disposed by conventional routes to repositories, but lends itself to consideration of alternative destinies such as thermal or chemical treatments applied to graphite in order to reduce dominant isotope content [67–71], as an example, Wigner energy becomes irrelevant if the graphite is thermally treated as part of a comprehensive disposal strategy. Whereas it is generally planned now to remove graphite from the majority of reactors as intact blocks, the effects of irradiation, combined with the presence in some cases of metallic components (pins, wires) within the structures, may make the consideration of alternative newly developed disposal strategies viable.

Advances in the treatment of graphite and carbowastes

Recently advances in the treatment of graphite waste have been made with international research programmes including EURATOM Framework Programme (CARBOWASTE: FP7-211333) [72] and IAEA Coordinated Research Programme [73] in order to establish best practices in the retrieval, treatment and disposal of irradiated graphite and other carbonaceous waste.

Thermal treatment is a promising alternative graphite waste management solution to allow separation of mobile radioactive isotopes such as ^{3}H, ^{14}C and ^{36}Cl from the bulk material, allowing for possible graphite higher activity waste volume reduction and concentration, and potential considerable cost saving. Gasification, pyrolysis and fluidized bed steam reforming are processes which are in widespread use in the chemical process / waste management industries. Applications include biomass gasification, metal reduction, chemical processes, petroleum refinery applications, and organic liquor destruction / energy recovery in the pulp and paper industry. These treatment techniques have been further developed for specific use with radioactive wastes because of their inherent capability to reduce the volume of waste requiring disposal and to form an inert, safe and stable waste suitable for disposal. One of the most technology advanced steam reforming processes for the gasification of graphite was THOR pyrolysis/steam reforming process [68]. However, the industrial feasibility of this treatment to graphite is not yet certain (R&D phase), and in comparison to oxygen treatment systems, the removal rates are 10 to 20 times slower. A further issue for the pyrolysis/steam reforming process is the requirement of high temperatures for gasification (>1100 °C), as shown in Figure 26.

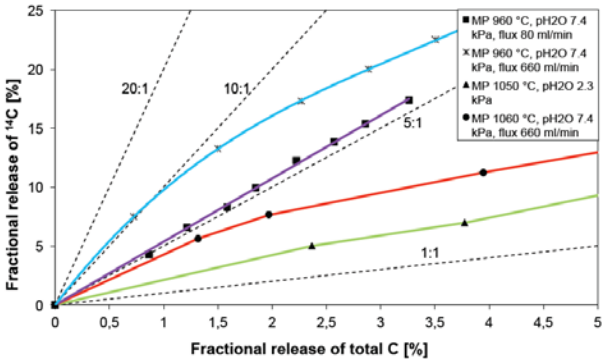

Figure 26 **Thermal treatment of graphite under steam conditions** [74]

At these high temperatures, volatile isotopes including ^{14}C, ^{3}H and ^{36}Cl, ^{134}Cs, ^{137}Cs; ^{90}Sr; ^{152}Eu are released into the gas phase and mixed with carbon dioxide. During gasification, radioactive elements remain with the non-volatile portion of the graphite or these may vaporise, depending on the volatility of the elements. Any gaseous radioactive elements condense onto larger particles in the waste stream, which are removed by the off-gas cleaning system, or nucleate and form sub-micron aerosols of their own. These sub-micron aerosol particles and gaseous radionuclides such as ^{3}H and ^{14}C can often penetrate the off-gas cleaning system equipment. For these reasons, the gasification of graphite may be contested as a viable treatment option. A comprehensive understanding of the influence of the gasification furnace operating parameters, such as the temperature and the gaseous composition, on the behaviour of the radioactive elements in the nuclear graphite waste can solve this problem.

Previous HTR treatment trial tests have shown the clean separation of HRT tristructural-isotropic (TRISO) fuel particles from the graphite matrix is possible at laboratory scale, at room temperature by acid treatment with a mixture of sulfuric acid and hydrogen peroxide. This treatment induces a delamination of the graphite layers and prevents damage of the particles, which constitutes the condition sine qua non for the success of the separation method applied to the spent TRISO fuel particles [75].

Molten Salt Reactors - Graphite

As well as considering the same graphite issues as for HTR core design MSR graphite technology has to consider issues related to the intimate contact between the graphite and molten salt fuel/coolant. The graphite in a thermal molten salt reactor (MSR) must have a microstructural porosity that can acheive two somewhat opposing requirements: i) the graphite should ideally exclude the molten salt fuel to prevent local overheating within the graphite porosity, and ii) the graphite must also as far as possible allow the removal of ^{135}Xe gas to reduce fission-product poisoning. This requires the internal graphite porosity to have pore diameters (as measured using mercury porosity), greater than 1µm to allow for the removal of ^{135}Xe and a pore diameter requirement of less than 100 nm to exclude the molten salt fuel and a helium diffusion coefficient of 10^{-8} m^2 s^{-1} and 10 nm [76]. Scott and Eatherly [77] in 1969 reviewed the requirements for graphite in a MSR concluding that the then

existing graphite grades could be utilised in a MSR core to give a life of about four years. This study also concluded that xenon could be removed by sparging the molten fuel salt with helium bubbles and removing them after enrichment. More recently the renewed interest in MSR technology [6] has given rise to the investigation of new graphite grades and possible graphite coatings [76,78,79]; these new materials are yet to be tested in an irradiated environment.

Discussion and conclusions

The use of graphite as a nuclear moderator has a long history due to its unique characteristics. It has been successfully deployed in numerous reactor generations, and not surprisingly it is currently a candidate for future Generation IV HTR and MSR reactors. Therefore, a fundamental understanding of its properties is of high importance to reactor designers.

This chapter presented the basics of graphite as a nuclear material based on experience in current graphite moderated reactors (Magnox, AGRs, and new candidate HTR material). Graphite properties are fascinating; not only do they differ dramatically at different scales, but they are different according to manufacture, mixture, grain size, and operational environment to name a few. Although this is generally beneficial, it makes it harder for the reactor designer/assessor to predict the future behaviour of graphite for reactor life extension, for example. However, despite all this variability, the trends of property changes in different graphite grades have shown commonalities to a certain degree. It was shown that the graphite grades that are candidates for Generation IV reactors behave in a similar way to the Gilsocarbon graphite used in the UK AGRs. Some initial models of most relevant material properties are provided along with current understanding of the causes of the property changes due to irradiation. Current procedures of assessing the graphite structural integrity are also presented as they are applicable to Generation IV. There is a large scope for improving the models and understanding the microstructural causes of the material changes due to irradiation. This eventually will lead to better design and longer life of a very stable reactor.

The authors also draw attention to specific issues related to high temperature graphite moderated reactors such as thermal oxidation in the event of an accident. Oxidation represents the lose mass of graphite, which if signification could limit its ability to moderate the fast neutrons. Thermal oxidation is not a problem in the current reactors such as the AGRs. However, current reactors suffer from a different type of oxidation, namely; radiolytic oxidation. This type of oxidation is not relevant to Genration IV, because the proposed cooling composition is inert.

The journey of using graphite as a moderator does not end at the final shut-down of the reactor. Regulatory bodies generally request viable and effective decommissioning plans from the design stage and certainly before an approval is granted. Therefore, current methods and plans of dealing with nuclear graphite waste are presented. Again, there is a large scope for improving or developing pioneering procedures and conditioning methods to deal with any future graphite waste.

References

[1] M.J. Kania, H. Nabielek, K. Verfondern, H.J. Allelein, Testing of HTR UO2 TRISO fuels in AVR and in material test reactors, J. Nucl. Mater. 441 (2013) 545–562. doi:10.1016/j.jnucmat.2013.05.062.

[2] W. Bernnat, W. Feltes, Models for reactor physics calculations for HTR pebble bed modular reactors, Nucl. Eng. Des. 222 (2003) 331–347. doi:10.1016/S0029-5493(03)00036-0.

[3] Z. Zhang, Z. Wu, D. Wang, Y. Xu, Y. Sun, F. Li, et al., Current status and technical description of Chinese 2 x 250MWth HTR-PM demonstration plant, Nucl. Eng. Des. 239 (2009) 1212–1219. doi:doi: 10.1016/j.nucengdes.2009.02.023.

[4] R. Hino, M.A. Fütterer, Y. Hassan, Special edition on HTR 2012 conference, Nucl. Eng. Des. 271 (2014) 1. doi:http://dx.doi.org/10.1016/j.nucengdes.2014.02.001.

[5] B.T. Kelly, P.A. V Johnson, P. Schofield, J.E. Brocklehurst, M. Birch, UKAEA Northern Division studies of the radiolytic oxidation of graphite in carbon dioxide, Carbon N. Y. 21 (1983) 441–449.

[6] D. LeBlanc, Molten salt reactors: A new beginning for an old idea, Nucl. Eng. Des. 240 (2010) 1644–1656. doi:10.1016/j.nucengdes.2009.12.033.

[7] National Institute of Standards and Technology, Neutron scattering lengths and cross sections, (n.d.). https://www.ncnr.nist.gov/resources/n-lengths/.

[8] A.J. Wickham, B.J. Marsden, Characterisation, Treatment and Conditioning of Radioactive Graphite from Decommissioning of Nuclear Reactors, IAEA TECDOC-1521,. (2006).

[9] B.J. Marsden, G.N. Hall, Graphite in gas-cooled reactors, in: Compr. Nucl. Mater., 1st ed., Elsevier Inc., 2012: pp. 325–390. doi:10.1016/B978-0-08-056033-5.00092-6.

[10] B.J. Marsden, G.N. Hall, 4.11 Graphite in Gas-Cooled Reactors BT - Reference Module in Materials Science and Materials Engineering, in: Elsevier, 2016. doi:http://dx.doi.org/10.1016/B978-0-12-803581-8.00729-3.

[11] H. Li, A.S.L. Fok, B.J. Marsden, An analytical study on the irradiation-induced stresses in nuclear graphite moderator bricks, J. Nucl. Mater. 372 (2008) 164–170. doi:10.1016/j.jnucmat.2007.03.041.

[12] R.E. Nightingale, Nuclear graphite., Academic Press, New York and London, 1962.

[13] S. Mrozowski, Mechanical strength, thermal expansion and structure of cokes and carbons, in: 1st 2nd Conf. Carbon, University of Buffalo, Buffalo, New York, 1956: pp. 31–45. doi:papers://D9F9AA35-5CC8-482E-89C5-625C9FC6984D/Paper/p2585.

[14] ASTM, Standard Specification for Isotropic and Near-isotropic Nuclear Graphites, (2014). doi:10.1520/D7219-08R14.

[15] ASTM, Standard Terminology Relating to Manufactured Carbon and Graphite, (2009).

[16] W.C. Morgan, Nuclear Fluence and atomic displacment rates for graphite irradiations, Nucl. Technol. 21 (1974).

[17] E.D. Eason, G. Hall, B.J. Marsden, Development of a model of dimensional change in AGR graphites irradiated in inert environments., in: G.B. Neighbour (Ed.), Conf. Ageing Manag. Graph. React. Cores, University of Cardiff, Wales, 2005: pp. 43–50.

[18] M. Bradford, A. Steer, A structurally-based model of irradiated graphite properties, J. Nucl. Mater. 381 (2008) 137–144. doi:10.1016/j.jnucmat.2008.07.040.

[19] D.K.L. Tsang, B.J. Marsden, S.L. Fok, G. Hall, Graphite thermal expansion relationship for different temperature ranges, Carbon N. Y. 43 (2005) 2902–2906.

[20] J.E. Brocklehurst, B.T. Kelly, The dimensional changes of highly-oriented pyrolytic graphite irradiated with fast neutrons at 430°C and 600°C, Carbon N. Y. 31 (1993) 179–183.

[21] R. Taylor, K.E. Gilchrist, L.J. Poston, Thermal conductivity of polycrystalline graphite, Carbon N. Y. 6 (1968) 537–544. doi:doi: DOI: 10.1016/0008-6223(68)90093-6.

[22] P.A. Thrower, The study of defects in graphite by transmission electron microscopy, Chem. Phys. Carbon. 5 (1969) 217–319.

[23] G. Hall, B.J. Marsden, S.L. Fok, The microstructural modelling of nuclear grade graphite, J. Nucl. Mater. 353 (2006) 12–18. doi:10.1016/j.jnucmat.2006.02.082.

[24] J. Lord, M. Lodeiro, G. Klimaytys, R. Morrel, J. Jiang, Experimental study of the Poisson's ratio of graphite, Graph. Res. Meet. (2008).

[25] T. Oku, M. Eto, A Relation Between Static and Dynamic Young's Moduli of Nuclear Graphites, Ibaraki Daigaku Kogakubu Kenkyu Shuho (Journal Fac. Eng. Ibaraki Univ. 39 (1991) 45–52.

[26] C. Berre, Microstructural Modelling of Nuclear Graphite, PhD Thesis, University of Manchester, 2007.

[27] H.H.W. Losty, J.S. Orchard, The Strength of Graphite, in: Fifth Carbon Conf., 1961.

[28] A.A. Griffith, The Phenomena of Rupture and Flow in Solids, Philos. Trans. R. Soc. London A Math. Phys. Eng. Sci. 221 (1921) 163–198. http://rsta.royalsocietypublishing.org/content/221/582-593/163.abstract.

[29] B.J. Marsden, S.L. Fok, T.J. Marrow, P.M. Mummery, The relationship between strength and modulus in nuclear graphite, HTR-2004, 2nd Int. Top. Meet. High Temp. React. Technol. (n.d.).

[30] H.H.W. Losty, J.S. Orchard, The strength of graphite, in: Fifth Conf. Carbon, Pergamon Press, Pennsylvania State University, University Park, Pennsylvania, 1962: pp. 519–532.

[31] B.T. Kelly, J.E. Brocklehurst, UKAEA Reactor Group studies of irradiation-induced creep in graphite, J. Nucl. Mater. 65 (1977) 79–85.

[32] G. Haag, Properties of ATR-2E graphite and property changes due to fast neutron irradiation, (2005).

[33] R.J. Price, Irradiation-induced creep in graphite: a review, (1981).

[34] B.T. Kelly, A. Foreman, Theory of irradiation creep in reactor graphite - dislocation pinning-unpinning model, Carbon N. Y. 11 (1973) 694.

[35] G.S. Was, Fundamentals of radiation materials science : metals and alloys, Springer, Berlin, 2007.

[36] C.R. Kennedy, M. Cundy, G. Kleist, The irradiation creep characteristics of graphite to high fluences, in: Carbon '88, Institute of Physics, Newcastle upon Tyne, UK, 1988: pp. 443–445.

[37] J.E. Brocklehurst, B.T. Kelly, A review of irradiation induced creep in graphite under CAGR conditions UKAEA Report ND-R1406, (1989).

[38] M.A. Davies, M. Bradford, A revised description of graphite irradiation induced creep, J. Nucl. Mater. 381 (2008) 39–45. doi:10.1016/j.jnucmat.2008.07.019.

[39] H. Wang, X. Zhou, L. Sun, J. Dong, S. Yu, The effect of stress levels on the coefficient of thermal expansion of a fine-grained isotropic nuclear graphite, Nucl. Eng. Des. 239 (2009) 484–489. doi:10.1016/j.nucengdes.2008.11.004.

[40] B.S. Gray, J. Brocklehurst, A.A. McFarlane, The irradiation induced plasticity in graphite under constant stress, Carbon N. Y. 5 (1967) 173–180.

[41] S.D. Preston, B.J. Marsden, Changes in the coefficient of thermal expansion in stressed Gilsocarbon graphite, Carbon N. Y. 44 (2006) 1250–1257. doi:10.1016/j.carbon.2005.10.045.

[42] D.K.L. Tsang, B.J. Marsden, The development of a stress analysis code for nuclear graphite components in gas-cooled reactors, J. Nucl. Mater. 350 (2006) 208–220. doi:10.1016/j.jnucmat.2006.01.015.

[43] D.K.L. Tsang, B.J. Marsden, Constitutive material model for the prediction of stresses in irradiated anisotropic graphite components, J. Nucl. Mater. 381 (2008) 129–136. doi:10.1016/j.jnucmat.2008.07.025.

[44] O.C. Zienkiewicz, R.L. Taylor, The Finite Element Method, Butterworth-Heinemann, 1986.

[45] J. Walker P.L., J. Rusinko Frank, L.G. Austin, Gas Reactions of Carbon, in: E. D.D. P.W. Selwood and Paul B. Weisz (Ed.), Vol. 11, Academic Press, 1959: pp. 133–221. doi:doi: DOI: 10.1016/S0360-0564(08)60418-6.

[46] P. Hawtin, J.A. Gibson, R. Murdoch, J.B. Lewis, The effect of diffusion and bulk gas flow on the thermal oxidation of nuclear graphite-I. Temperatures below 500°C, Carbon N. Y. 2 (1964) 299–309. doi:10.1016/0008-6223(64)90044-2.

[47] E. Loren Fuller, J.M. Okoh, Kinetics and mechanisms of the reaction of air with nuclear grade graphites: IG-110, J. Nucl. Mater. 240 (1997) 241–250. doi:10.1016/S0022-3115(96)00462-X.

[48] Graphite Oxidation Thermodynamics / Reactions, (1998) 32025899.

[49] L. Xiaowei, R. Jean-Charles, Y. Suyuan, Effect of temperature on graphite oxidation behavior, Nucl. Eng. Des. 227 (2004) 273–280. doi:10.1016/j.nucengdes.2003.11.004.

[50] E.S. Kim, K.W. Lee, H.C. No, Analysis of geometrical effects on graphite oxidation through measurement of internal surface area, J. Nucl. Mater. 348 (2006) 174–180. doi:10.1016/j.jnucmat.2005.09.018.

[51] X. Luo, X. Yu, S. Yu, Oxidation performance of graphite material in reactors, Front. Energy Power Eng. China. 2 (2008) 471–474. http://dx.doi.org/10.1007/s11708-008-0074-6.

[52] C.I. Contescu, S. Azad, D. Miller, M.J. Lance, F.S. Baker, T.D. Burchell, Practical aspects for characterizing air oxidation of graphite, J. Nucl. Mater. 381 (2008) 15–24. doi:10.1016/j.jnucmat.2008.07.020.

[53] H.-K. Hinssen, K. Kühn, R. Moormann, B. Schlögl, M. Fechter, M. Mitchell, Oxidation experiments and theoretical examinations on graphite materials relevant for the PBMR, Nucl. Eng. Des. 238 (2008) 3018–3025. doi:doi: DOI: 10.1016/j.nucengdes.2008.02.013.

[54] IAEA - TECDOC-1154, Irradiation Damage in Graphite due to Fast Neutrons in Fission and Fusion Systems, TECDOC-1154, IAEA, 2000.

[55] M.S. El-Genk, J.-M.P. Tournier, Comparison of oxidation model predictions with gasification data of IG-110, IG-430 and NBG-25 nuclear graphite, J. Nucl. Mater. 420 (2012) 141–158. doi:10.1016/j.jnucmat.2011.09.027.

[56] J.J. Lee, T.K. Ghosh, S.K. Loyalka, Oxidation rate of nuclear-grade graphite NBG-18 in the kinetic regime for VHTR air ingress accident scenarios, J. Nucl. Mater. 438 (2013) 77–87. doi:10.1016/j.jnucmat.2013.03.002.

[57] R. Moormann, H.-K. Hinssen, K. Kuhn, Oxidation behaviour of an HTR fuel element matrix graphite in oxygen compared to a standard nuclear graphite, Nucl. Eng. Des. 227 (2004) 281–284.

[58] M.S. El-Genk, J.-M.P. Tournier, Development and validation of a model for the chemical kinetics of graphite oxidation, J. Nucl. Mater. 411 (2011) 193–207. doi:10.1016/j.jnucmat.2011.01.129.

[59] W.-K. Choi, B.-J. Kim, E.-S. Kim, S.-H. Chi, S.-J. Park, Oxidation behavior of IG and NBG nuclear graphites, Nucl. Eng. Des. 241 (2011) 82–87. doi:10.1016/j.nucengdes.2010.10.007.

[60] L. Payne, P.J. Heard, T.B. Scott, A Study of the Oxidation Behaviour of Pile Grade A (PGA) Nuclear Graphite Using Thermogravimetric Analysis (TGA), Scanning Electron Microscopy (SEM) and X-Ray Tomography (XRT), PLoS One. 10 (2015) 1–19. doi:10.1371/journal.pone.0143041.

[61] NDA Report SMS/TS/D1-HAW-6/002/A, Higher Activity Waste The Long-term Management of Reactor Core Graphite Waste Credible Options, 2013.

[62] NDA, Radioactive Wastes in the UK: A Summary of the 2010 Inventory, (2010). doi:978-1-905985-20-3.

[63] B.J. Marsden, A.J. Wickham, Graphite disposal options - A comparison of the approaches proposed by UK and Russian reactor operators, in: Nucl. Decommissioning 1998, Professional Engineering Publishing, London, 1998: pp. 145–153.

[64] A.J. Wickham, UK Nuclear Graphite Decommissioning, (2008).

[65] A.N. Jones, B.J. Marsden, Review of the Characterisation of Nuclear Graphites in UK Reactors Scheduled for Decommissioning, IAEA-TECDOC-1647. 06. (2010) 30.

[66] M.P. Metcalfe, R.W. Mills, Radiocarbon mass balance for a Magnox nuclear power station, Ann. Nucl. Energy. 75 (2015) 665–671. doi:http://dx.doi.org/10.1016/j.anucene.2014.08.071.

[67] M.P. Metcalfe, A.W. Banford, H. Eccles, S. Norris, EU Carbowaste project: Development of a toolbox for graphite waste management, J. Nucl. Mater. 436 (2013) 158–166. doi:10.1016/j.jnucmat.2012.11.016.

[68] J.B. Mason, D. Bradbury, A.J. Wickham, J. Buffery, J. Fachinger, Pyrolysis / Steam Reforming and its Potential Use in Graphite Disposal, in: EPRI (Ed.), Proc. 3rd EPRI Int. Decommissioning Radioact. Waste Work., IAEA, Lyon, France, 2004: pp. 77–84.

[69] J. Fachinger, 14C and 3H Thermal Treatment from Merlin Graphite, CARBOWASTE 2nd Annu. Steer. Comm. Meet. (2009).

[70] J.R. Costes, C. de Tassigny, H. Vidal, Conditioning graphite bricks from dismantled gas-cooled reactors for disposal, Waste Manag. 10 (1990) 297–302.

[71] M. Lou Dunzik-Gougar, T.E. Smith, Removal of carbon-14 from irradiated graphite, J. Nucl. Mater. 451 (2014) 328–335. doi:10.1016/j.jnucmat.2014.03.018.

[72] W. von Lensa, CARBOWASTE: New EURATOM Project on "Treatment and Disposal of Irradiated Graphite and other Carbonaceous Waste," Proc. 4th Int. Top. Meet. High-Temperature React. Technol. (2008).

[73] IAEA, Treatment of Irradiated Graphite to Meet Acceptance Criteria for Waste Disposal, T21026. ACTIVE (2010).

[74] W. von Lensa, A.N. Jones, D. Vulpius, A. Banford, Treatment and Disposal of irradiated Graphite and other Carbonaceous Waste, ATW - Int. J. Nucl. Power. 56 (2011) 263.

[75] J. Palosaari, R. Latonen, J. Smått, R. Blomqvist, O. Eklund, High-quality flake graphite occurrences in a high-grade metamorphic region in Sortland , 96 (2016) 19–26.

[76] J. Song, Y. Zhao, J. Zhang, X. He, B. Zhang, P. Lian, et al., Preparation of binderless nanopore-isotropic graphite for inhibiting the liquid fluoride salt and Xe135 penetration for molten salt nuclear reactor, Carbon N. Y. 79 (2014) 36–45. doi:10.1016/j.carbon.2014.07.022.

[77] D. Scott, W.P. Eatherly, Graphite and Xenon Behavior and Their Influence on Molten-Salt Reactor Design, Nucl. Appl. Technol. 8 (1970) 179–189.

[78] X. He, J. Song, J. Tan, B. Zhang, H. Xia, Z. He, et al., SiC coating: An alternative for the protection of nuclear graphite from liquid fluoride salt, J. Nucl. Mater. 448 (2014) 1–3. doi:10.1016/j.jnucmat.2014.01.034.

[79] V. Bernardet, S. Gomes, S. Delpeux, M. Dubois, K. Guérin, D. Avignant, et al., Protection of nuclear graphite toward fluoride molten salt by glassy carbon deposit, J. Nucl. Mater. 384 (2009) 292–302. doi:10.1016/j.jnucmat.2008.11.032.